Article

TRANSPARENT PROCESS

THE EMBO JOURNAL

Endosome maturation factors Rabenosyn-5/VPS45 and caveolin-1 regulate ciliary membrane and polycystin-2 homeostasis

Noémie Scheidel*, Julie Kennedy & Oliver E Blacque**

Abstract

Primary cilium structure and function relies on control of ciliary membrane homeostasis, regulated by membrane trafficking processes that deliver and retrieve ciliary components at the periciliary membrane. However, the molecular mechanisms controlling ciliary membrane establishment and maintenance, especially in relation to endocytosis, remain poorly understood. Here, using *Caenorhabditis elegans*, we describe closely linked functions for early endosome (EE) maturation factors RABS-5 (Rabenosyn-5) and VPS-45 (VPS45) in regulating cilium length and morphology, ciliary and periciliary membrane volume, and ciliary signalling-related sensory behaviour. We demonstrate that RABS-5 and VPS-45 control periciliary vesicle number and levels of select EE/endocytic markers (WDFY-2, CAV-1) and the ciliopathy membrane receptor PKD-2 (polycystin-2). Moreover, we show that CAV-1 (caveolin-1) also controls PKD-2 ciliary levels and associated sensory behaviour. These data link RABS-5 and VPS-45 ciliary functions to the processing of periciliary-derived endocytic vesicles and regulation of ciliary membrane homeostasis. Our findings also provide insight into the regulation of PKD-2 ciliary levels via integrated endosomal sorting and CAV-1-mediated endocytosis.

Keywords caveolin-1; cilia; PKD2; Rabenosyn-5; VPS45
Subject Categories Membrane & Intracellular Transport
DOI 10.15252/embj.201798248 | Received 15 September 2017 | Revised 8 February 2018 | Accepted 16 February 2018 | Published online 23 March 2018
The EMBO Journal (2018) 37: e98248

Introduction

Cilia are microtubule-based organelles enveloped by a specialised ciliary membrane that extend from the surface of most eukaryotic cell types. Whereas motile cilia propel cells through fluids and regulate fluid flow across tissues, motile and non-motile (primary) cilia act as cellular antennae, transducing extracellular physico-chemical signals associated with phototransduction, mechanosensation, thermosensation, olfaction and gustation (Satir *et al*, 2010). Primary cilia are also critical relays of developmental cell–cell communication signals such as Sonic Hedgehog (Shh) that regulate cell fate and behaviour (Goetz & Anderson, 2010; Hilgendorf *et al*, 2016). Defects in cilia are linked to a large number of genetically inherited human diseases (ciliopathies) affecting most tissues, causing a pleiotropic phenotype that includes retinal dystrophy and degeneration, cystic kidneys, organ and bone patterning defects, nervous system impairment and obesity (Waters & Beales, 2011; Reiter & Leroux, 2017).

The ciliary membrane is enriched for many different receptors, channels and signal transducers including TRP channels linked to cystic kidney disease (e.g. polycystin-1/2), cell–cell communication regulators (e.g. Shh) and a large number of G protein-coupled receptors (GPCRs) (e.g. Rhodopsin, 5HT6; Goetz & Anderson 2010; Kathem *et al*, 2014; McIntyre *et al*, 2016; Hilgendorf *et al*, 2016). The ciliary membrane also has a specialised lipid composition that includes specific phosphoinositides essential for normal ciliary structure and function (Jacoby *et al*, 2009; Chávez *et al*, 2015; Garcia-Gonzalo *et al*, 2015; Dyson *et al*, 2017). The importance of the ciliary membrane for signalling is highlighted by the Shh pathway, wherein Shh activation causes transmembrane Ptch1 to exit the cilium, concomitant with the ciliary entry of the downstream pathway activator, Smo (Corbit *et al*, 2005; Rohatgi *et al*, 2007; Milenkovic *et al*, 2009; Schou *et al*, 2015). Thus, cilium-based signalling requires regulated and dynamic delivery and removal of signal transducers, and is therefore reliant on mechanisms that control ciliary protein and membrane composition.

The formation and function of cilia is highly dependent on protein and membrane trafficking pathways, together with gating and shedding mechanisms at the ciliary base and tip, respectively. Intraflagellar transport (IFT), consisting of kinesin-2 and IFT-dynein motors as well as cargo adaptor complexes (IFT-A, IFT-B, BBSome), moves bidirectionally between the ciliary base and tip, and regulates the ciliary entry, removal and distribution of various proteins (Rosenbaum & Witman, 2002; Lechtreck, 2015; Jensen & Leroux, 2017). For ciliary membrane proteins, at least three routes are proposed for their delivery to the periciliary membrane region at the ciliary base: (i) direct trafficking and docking of TGN-derived vesicles at the periciliary membrane (Papermaster *et al*, 1985; Deretic *et al*, 1995; Deretic, 2013; Vetter *et al*, 2015; Monis *et al*, 2017), (ii) vesicular

UCD School of Biomolecular and Biomedical Science, University College Dublin, Dublin 4, Ireland
*Corresponding author. Tel: +353-1-7166953; E-mail: noemie.scheidel@ucdconnect.ie
**Corresponding author. Tel: +353-1-7166953; E-mail: oliver.blacque@ucd.ie

transport to the plasma membrane, followed by lateral diffusion to the periciliary membrane (Hunnicutt, 1990; Milenkovic *et al*, 2009; Cao *et al*, 2015), and (iii) endocytosis at the plasma membrane, and subsequent endosomal sorting and recycling to the periciliary membrane (Nachury *et al*, 2010; Malicki & Avidor-Reiss, 2014; Jensen & Leroux, 2017; Monis *et al*, 2017; Mukhopadhyay *et al*, 2017). For some proteins, translocation into and out of the cilium is restricted by bidirectional membrane and cytosolic diffusion barriers ("gates") at the proximal-most part of the ciliary axoneme, within the transition zone (TZ) and transition fibre regions, and mechanisms to overcome these transport barriers include IFT and lipidated protein intraflagellar targeting (LIFT) (Nachury *et al*, 2010; Reiter *et al*, 2012; Szymanska & Johnson, 2012; Wätzlich *et al*, 2013; Malicki & Avidor-Reiss, 2014; Ismail, 2016; Jensen & Leroux, 2017). Finally, ciliary membrane homeostasis is also regulated by a protein turnover mechanism involving ectosome release from the ciliary tip (Wood & Rosenbaum, 2015; Wang & Barr, 2016; Nager *et al*, 2017; Phua *et al*, 2017).

Multiple lines of evidence implicate important roles for endocytic regulators in cilium formation and resorption, and the control of ciliary signalling and membrane homeostasis. In protist and mammalian cells, an invagination of the plasma membrane from where the cilium emerges called the ciliary (or flagellar) pocket contains clathrin-coated pits, and various endocytic and early endosomal machinery such as clathrin, the AP-2 adaptor, and RAB5 (Field & Carrington, 2009; Molla-Herman *et al*, 2010; Rattner *et al*, 2010; Benmerah, 2013; Clement *et al*, 2013; Saito *et al*, 2017; Schou *et al*, 2017). Similarly, we and others observe various endocytic regulators (clathrin, AP-2 adaptor, dynamin, RAB5, STAM1, Hrs) within the *Caenorhabditis elegans* periciliary membrane compartment (PCMC), which shares some similarities with the ciliary pocket (Hu *et al*, 2007; Kaplan *et al*, 2012; van der Vaart *et al*, 2015; Jensen & Leroux, 2017). Functionally, mammalian RAB5 and clathrin-mediated endocytosis (CME), as well as the endocytic recycling protein EHD1 and the caveolin component CAV1, are associated with TGF-beta and Shh signalling in the cilium (Clement *et al*, 2013; Schou *et al*, 2015; Pedersen *et al*, 2016). In *C. elegans*, CME facilitates ciliary and periciliary membrane retrieval via a mechanism counter-balanced by BBS-8- and RAB-8-mediated membrane delivery (Kaplan *et al*, 2012). *Caenorhabditis elegans* CME and endosomal sorting machinery (STAM, Hrs) also regulate the localisations of multiple ciliary membrane signalling molecules, including the polycystin-2 orthologue (PKD-2) that controls male mating behaviour (Hu *et al*, 2007; Kaplan *et al*, 2012; O'Hagan *et al*, 2014).

To shed light on the poorly understood mechanisms underpinning ciliary membrane homeostasis, we performed a reverse genetics screen of known membrane trafficking regulators and identified novel cilium structure and function roles for the *C. elegans* orthologues of endosome maturation factors, Rabenosyn-5 (RABS-5) and VPS45 (VPS-45). Both proteins regulate ciliary and periciliary membrane structure, PCMC vesicle number, PKD-2 localisation and male mating behaviour. We also identify enriched pools of WDFY-2-associated early endosomes (EE) and CAV-1 (caveolin-1 orthologue) at the ciliary base, and show that their PCMC levels are dependent on RABS-5 and VPS-45. In addition, we provide evidence that CAV-1 also regulates PKD-2 ciliary localisation and related mating behaviours. Our findings suggest that RABS-5 and VPS-45 function together to regulate the fusion and maturation of specific cilium-derived endocytic vesicles and EEs. Our data also implicate a role for caveolin-1-regulated endocytosis in controlling ciliary membrane composition and associated signalling.

Results

A reverse genetic screen identifies cilium structure/function roles for *Caenorhabditis elegans* Rabenosyn-5 (RABS-5)

To identify new regulators of ciliary membrane trafficking, we employed a reverse genetics approach in *Caenorhabditis elegans* to screen mutant alleles of conserved candidate genes for cilium structure and function defects (Fig 1A). Candidate genes were selected from: (i) large data sets of membrane trafficking regulators (Simpson *et al*, 2012) and (ii) literature mining for regulators of membrane organisation and homeostasis. In total, we identified 44 candidates with an unambiguous orthologue in *C. elegans* (bidirectional top hit), and for which predicted loss of function or null alleles (deletions, early stops) were available (Appendix Table S1). Cilium structure was assessed using dye-filling, which reports on the structural integrity of six pairs of environmentally exposed amphid cilia in the head and both pairs of phasmid cilia in the tail (Perkins *et al*, 1986; Starich *et al*, 1995). Cilium function was examined using two assays of sensory behaviour: (i) food foraging activity (roaming), which relies on multiple ciliated sensory neuronal inputs, and (ii) osmotic avoidance to a hypertonic environment (Osm), mediated by the ASH neuron (Colbert *et al*, 1997; Fujiwara *et al*, 2002; Liedtke *et al*, 2003; Solomon, 2004; Sanders *et al*, 2015).

From this screen, we identified dye-filling and roaming (but not Osm) defects for a mutant allele (*ok1513*) of *rabs-5* (Figs 1B and C, and EV1A and B), which is the orthologue of the Rab5 effector, Rabenosyn-5, that regulates early endosome maturation and protein sorting towards lysosomal degradation and recycling (Nielsen *et al*, 2000; Gengyo-Ando *et al*, 2007; Morrison *et al*, 2008). The *rabs-5 (ok1513)* roaming and dye-filling defects are rescued by transgenic expression of wild-type *rabs-5* genomic sequences under the control of an *arl-13* promoter active solely in ciliated neurons (Cevik *et al*, 2013), indicating that RABS-5 regulates these phenotypes by functioning in ciliated cells (Fig 1B and C).

Since dye-filling is an indirect measure of cilium structure, we directly examined amphid and phasmid channel cilium structure, morphology and compartmentalisation in *rabs-5* worms using fluorescent protein-tagged reporters that label the entire cilium and basal body (XBX-1), middle segment (ARL-13), transition zone (MKS-2) or PCMC (RPI-2, TRAM-1) (Schafer *et al*, 2003; Blacque *et al*, 2005; Cevik *et al*, 2010; Williams *et al*, 2011). We also examined AWB and OLQ cilia morphologies using *str-1*p::GFP and OSM-9::GFP reporters, respectively (Colbert *et al*, 1997; Troemel *et al*, 1999). We found that *rabs*-5 worms possess truncated phasmid, AWB and OLQ cilia, as well as a truncated ARL-13 compartment (phasmid cilia) (Figs 1D–F and EV1C and D). Furthermore, *rabs-5* mutants display enlarged periciliary membrane compartments (PCMC), as well as abnormal AWB and OLQ ciliary membrane expansions (Fig 1D–F). In contrast, *rabs-5* loss does not affect the localisations of MKS-2, RPI-2 or TRAM-1, indicating that TZ composition and gating function is normal in these worms (Figs 1D and EV1D).

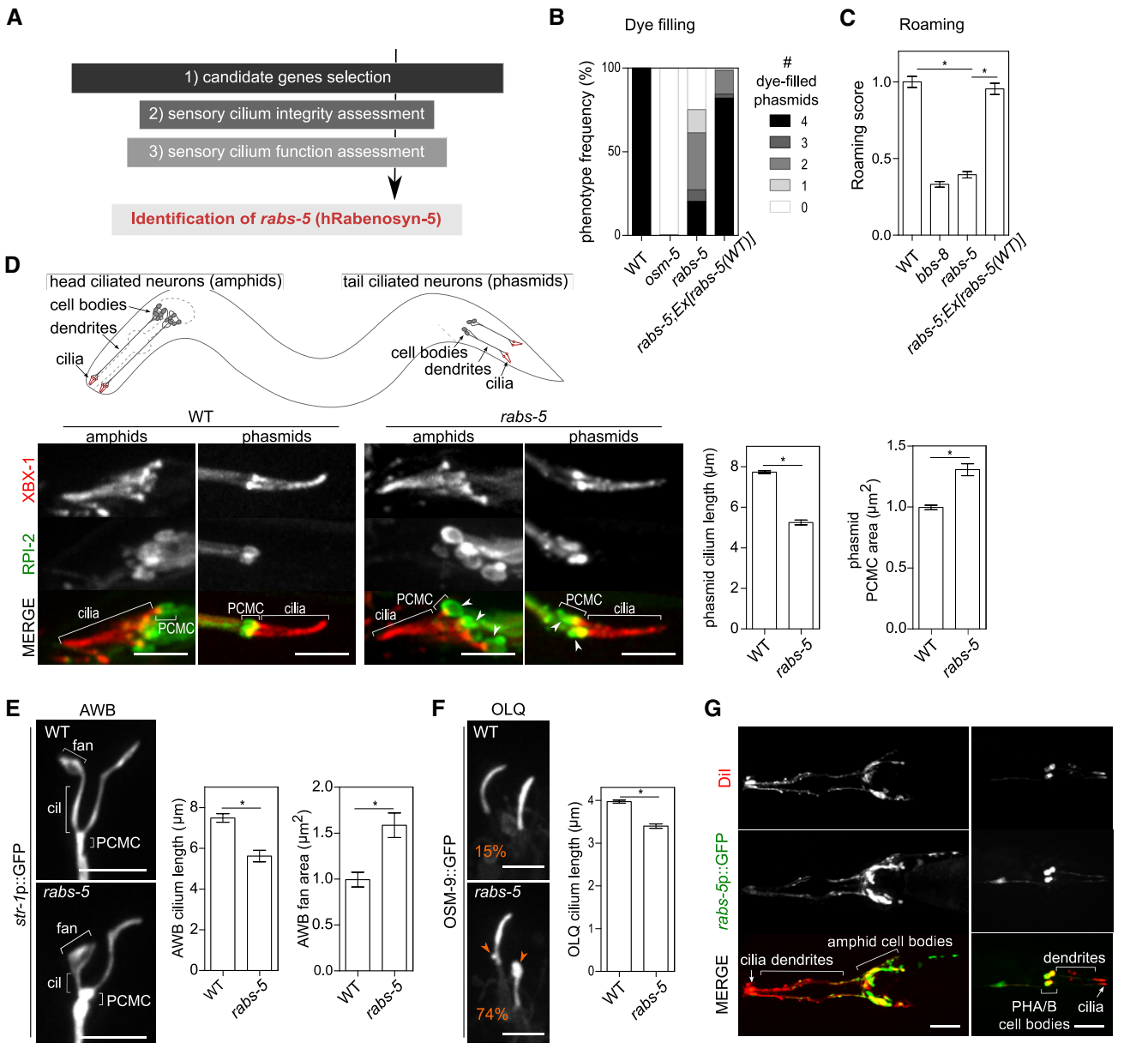

Figure 1. A reverse genetic screen identifies cilium structure and function defects in a mutant allele of *Caenorhabditis elegans* Rabenosyn-5 (*rabs-5*).

A Flow chart of reverse genetic screen to identify ciliary membrane homeostasis regulators.

B Quantification of DiI uptake in the phasmid neurons of the indicated genetic backgrounds. In each case, the number (0–4) of phasmid neurons taking up dye is scored. *osm-5(p813)* used as positive control. Bars show phenotype frequency (%) from four independent experiments ($n > 35$ per experiment).

C Quantification of roaming behaviour for the indicated genetic backgrounds. *bbs-8(nx77)* used as positive control. Bars show roaming score as mean ± SEM ($n = 60$). *$P < 0.001$ (unpaired Student's *t*-test; vs. WT or *rabs-5*).

D Representative images (Z-projects) and quantification of cilium length and PCMC area in WT and *rabs-5(ok1513)* worms expressing XBX-1::tdTomato (labels the ciliary axoneme) and RPI-2::GFP (labels the PCMC membrane; excluded from the ciliary membrane). White arrowhead indicates PCMC expansions. Bars in graphs show mean ± SEM ($n = 60$). *$P < 0.001$ (unpaired Student's *t*-test; vs. WT). Schematic shows location and organisation of amphid and phasmid ciliated neurons in *C. elegans*. Anterior is to the left (images). Scale bars = 5 µm.

E Representative images (Z-projects) and quantification of AWB cilium branch length and fan area in WT and *rabs-5(ok1513)* worms expressing a soluble GFP reporter (*str-1p::gfp*). Bars show mean ± SEM values ($n = 30$). *$P < 0.001$ (unpaired Student's *t*-test; vs. WT). Anterior is to the top (images). Cil, ciliary axoneme. Scale bars = 5 µm.

F Representative images (Z-projects) and quantification of OLQ cilium length in WT and *rabs-5(ok1513)* worms expressing the *osm-9::gfp* reporter. Bars show mean ± SEM ($n = 35$). *$P < 0.001$ (unpaired Student's *t*-test; vs. WT). Orange arrowheads indicate bulges in the ciliary membrane, and (%) in panel indicates the phenotype occurrence. Anterior is to the top (images). Scale bars = 3 µm.

G Representative images (Z-projects) of the head and tail regions of WT worms expressing a transcriptional GFP reporter for *rabs-5* (*rabs-5p::gfp*) and co-stained with DiI (stains six pairs of ciliated amphid neurons and the pair of ciliated phasmid neurons). GFP expressed in all dye-filling neurons. Anterior is to the left. Scale bars = 30 µm.

Although *ok1513* is likely a null allele, deleting 80% of *rabs-5* coding sequence (Fig 2A), this mutation causes developmental arrest at 25°C. Since the above data were generated at the permissive temperature (15°C), we examined possible temperature effects on the *rabs-5* ciliary phenotype. First, we found that adult *rabs-5* worms cultured at 20°C possess the same dye-filling and cilium structure phenotypes (axoneme length, PCMC size) as those cultured at 15°C (Fig EV1A and C). However, ciliary defects (dye-filling, phasmid cilium length, PCMC size) are somewhat more severe in worms subjected to a tolerated short period (24 h) of L4 stage growth at 25°C (Fig EV1A and C). Thus, growth at the restricted temperature modestly enhances the ciliary phenotype of *rabs-5(ok1513)* worms.

To examine whether RABS-5 functions to establish or maintain the ciliary compartment, we examined the ciliary phenotype of *rabs-5* mutants at different developmental stages, grown at 15°C or 20°C. We found that mutant larvae and adults possess a similar level of phasmid dye-filling and cilium length phenotype when compared to WT controls (Fig EV1A and C). Thus, RABS-5 functions during early stages of ciliary axoneme and membrane development. However, later maintenance functions are also probable, given our results with the temperature shift experiments described above (Fig EV1A and C).

These data reveal that *C. elegans* RABS-5 regulates the structure and function of multiple ciliary subtypes. A ciliary role for *rabs-5* also agrees with our finding that a GFP reporter under the control of 1,566 bp of *rabs-5* upstream regulatory sequence (*rabs-5*p::GFP) is expressed predominantly in ciliated cells, including all dye-filling amphid and phasmid neurons, male tail ray neurons and the PQR neuron (weaker expression) [Figs 1G and EV1E (whole-worm images)]. No apparent differences in *rabs-5*p::*gfp* expression were found in L1 vs. adult worms (Fig EV1E). It should be noted that our reporter may not have included all of the cis-regulatory *rabs-5* sequence. Indeed, *rabs-5* expression could be under additional cis-regulatory control as part of an operon with the upstream gene (Allen *et al*, 2011), thereby accounting for RABS-5 functions in additional non-ciliated cell types.

RABS-5 ciliary function and early endosome localisation depends on the FYVE domain

The *C. elegans* RABS-5 protein shows high sequence homology (72% amino acid similarity) to human Rabenosyn-5 and retains most of the domains found in the latter, namely an N-terminal C_2H_2 zinc-finger domain (ZnF), a FYVE membrane-binding domain that interacts with phosphatidylinositol 3-phosphate (PI3P) (Gaullier *et al*, 1998) and a C-terminal RAB protein-binding domain (RBD) (Eathiraj *et al*, 2005; Fig 2A). To investigate the requirement of these domains for RABS-5 ciliary functions, we constructed RABS-5 variants (RFP-tagged) lacking the ZnF, FYVE or RBD domains and assessed their abilities to rescue the dye-filling, cilium morphology and expanded PCMC phenotypes of the *rabs-5* mutant. We also examined whether these constructs rescue an OSM-6::GFP dendritic accumulation phenotype we observe in *rabs-5* mutant worms (Fig 2C). We found that the RABS-5(ΔZnF) and RABS-5(ΔRBD) constructs rescue all assayed *rabs-5* mutant phenotypes to the same extent as the RABS-5(WT) construct (Fig 2B–D). In contrast, the RABS-5(ΔFYVE) construct does not rescue *rabs-5* phenotypes (Fig 2B–D). Indeed, RABS-5(ΔFYVE) overexpression causes a partial reduction in dye-filling in wild-type worms, indicating that RABS-5 (ΔFYVE) exerts a dominant-negative effect on cilium integrity (Fig EV2A). Thus, RABS-5 regulation of cilium structure requires the PI3P-interacting FYVE domain, but not the ZnF and RAB binding domains.

Next, we investigated the subcellular localisations of the RFP-tagged RABS-5 wild-type and variant reporters in ciliated neurons, together with GFP::RAB-5, which is a marker of EEA-1-positive EEs (Mills *et al*, 1998; Patki *et al*, 1997; Simonsen *et al*, 1998; Fig EV2B). In hermaphrodites, the RABS-5(WT) reporter displays vesicular or EE-like signals in the cell bodies colocalised with

Figure 2. RABS-5 ciliary function and early endosome localisation is dependent on the FYVE domain.

A Schematics showing the domain organisation of human Rabenosyn-5 and *Caenorhabditis elegans* (*C. el.*) RABS-5. Note that the NPF and central RBD domains are absent in RABS-5. Striped region indicates the location of the *ok1513* deletion. Number in brackets indicates the amino acid (aa) length of the proteins.

B Quantification of DiI uptake in the phasmid neurons of WT and *rabs-5(ok1513)* mutant worms expressing the indicated RFP-tagged transgenes. In each case, the number (0–4) of phasmid neurons taking up dye is scored. Bars show phenotype frequency (%) from four independent experiments ($n > 35$ per experiment).

C Representative images of four phasmid cilia (2 pairs) from WT and *rabs-5(ok1513)* worms expressing OSM-6::GFP (IFT52 orthologue, decorates the cilium and dendritic compartments) and the indicated RFP-tagged transgenes. Arrowheads indicate expanded periciliary membrane compartments (PCMC). Star indicates OSM-6::GFP dendritic accumulation. Anterior is to the left. Scale bars = 5 μm

D Quantification of phasmid phenotypes in (C). Schematic shows the specific phenotypes scored as: (1) "WT like" (no ciliary morphology defects and no OSM-6::GFP accumulation along the dendrite), or (2) "Affected" (one or both phasmid pairs): ciliary morphology defects (left-hand graph, PCMC expansion and/or shorter axoneme) or OSM-6 accumulation in distal dendrite region (right-hand graph). Graphs show phenotype frequency (%) from three independent experiments ($n > 35$ per experiment).

E Subcellular localisation of RABS-5(WT) and RABS-5 variant reporters. Shown are representative images (Z-projects) of the phasmid neurons (PHA/B) of WT worms expressing the indicated reporters expressed in ciliated cells using *arl-13* promoter sequence. Left images show the PHA/B cell bodies (and PQR in the case of the RABS-5(ΔRBD) and RABS-5(ΔFYVE) images); right images show distal dendrite and ciliary regions. White arrowhead indicates RABS-5 colocalised with RAB-5 on vesicles. Unfilled arrowhead indicates RABS-5 vesicles uncoupled from RAB-5-positive early endosomes. PCMC, periciliary membrane compartment. Anterior is to the left. Scale bars = 5 μm.

F Quantification of localisation phenotypes in (E). Left graph quantifies RFP::RABS-5 and GFP::RAB-5 colocalisation in cell bodies. Data represented as mean ± SEM (6–12 independent experiments; number of vesicles counted indicated above each bar). Right graph quantifies the PCMC enrichment of the indicated RFP-tagged RABS-5 variant. Bars show mean ± SEM (n = 21–27 measurements per condition). *$P < 0.001$ [nonparametric Mann–Whitney *U*-test; vs. RABS-5(WT)]. EE, early endosomes.

G Representative images (Z-projects) of the head and tail regions of WT male worms expressing *pkd-2*p::*rfp*::*rabs-5* and *pkd-2*::*gfp*. PCMC, periciliary membrane compartment. Inset shows higher magnification images of the ciliary region of one pair of ray neurons. Anterior is to the top. Scale bars = 5.0 and 2.5 μm (insets).

H Schematic summarising the localisations of RABS-5 (denoted in red) in hermaphrodite and male-specific ciliated neurons. CB, cell bodies. PCMC, periciliary membrane compartment. EE, early endosome.

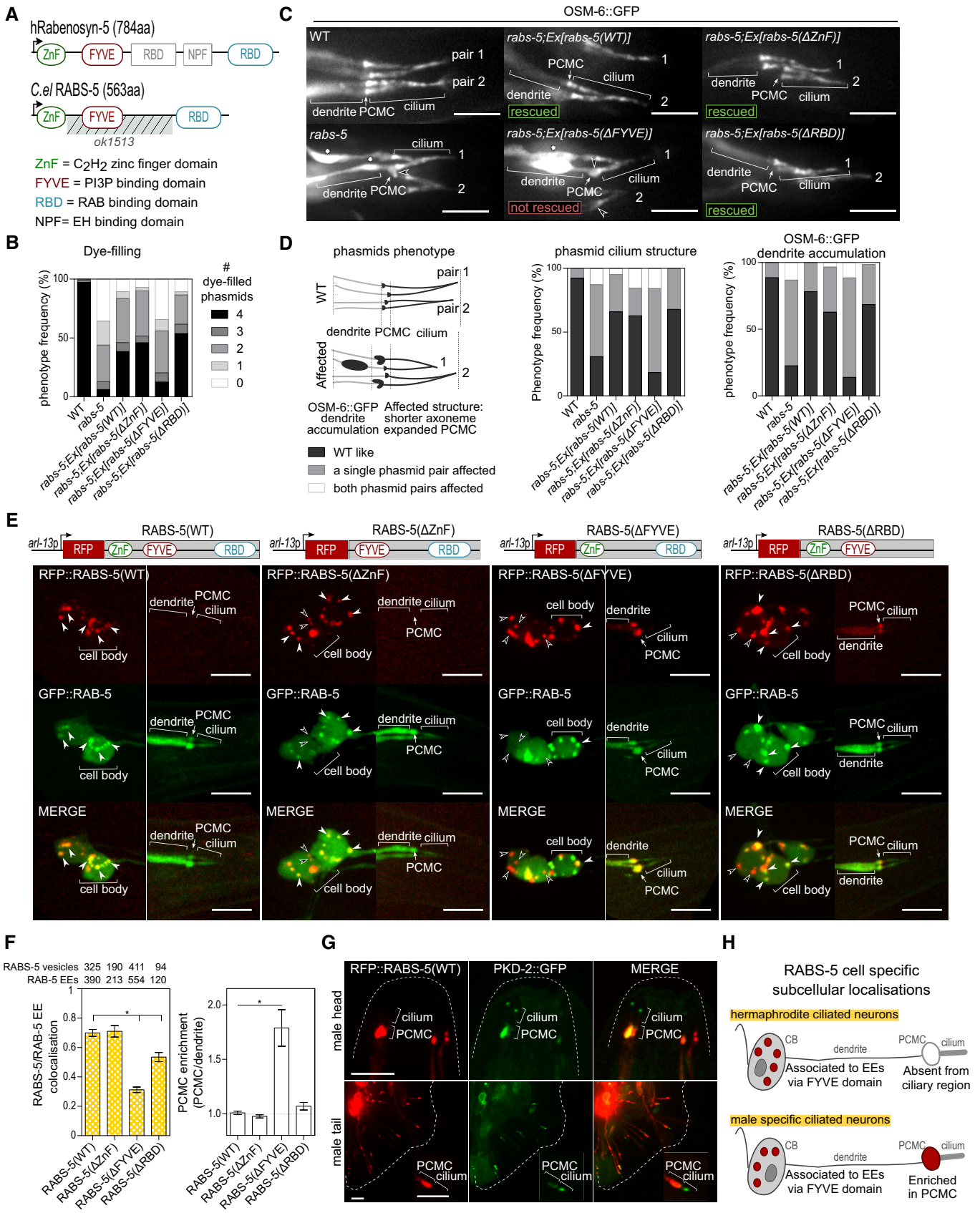

Figure 2.

RAB-5, but is absent from the dendrite and ciliary regions, including the PCMC [Figs 2E and F, and EV2C (whole-cell images)]. However, in male-specific head (CEM) and tail (ray) ciliated neurons, an enriched pool of RABS-5 occurs at the PCMC in addition to the cell bodies (Fig 2G). Thus, RABS-5 localises to EEs in ciliated neurons and displays a cell type-specific enrichment at the PCMC (Fig 2H). Analysis of the RABS-5 variants in hermaphrodites revealed that the RABS-5(ΔZnF) and RABS-5 (ΔRBD) localisations are comparable to RABS-5(WT), although RABS-5(ΔRBD) displays a slightly reduced RAB-5 colocalisation and is occasionally observed as a diffuse signal at the ciliary base [Figs 2E and F, and EV2C (whole neuron images)]. In contrast, RABS-5(ΔFYVE) localisation is altered compared to RABS-5(WT), displaying ectopic signals in the PCMC, association with large mobile vesicle-like structures in the dendrites, and cell body signals that are not colocalised with RAB-5 [Figs 2E and F, and EV2C (whole neuron images) and D, and Movie EV1]. Therefore, the abrogated function of RABS-5(ΔFYVE) correlates with a disrupted localisation for this RABS-5 variant in ciliated neurons (Fig 2H).

Collectively, our data indicate that RABS-5, via its FYVE membrane-binding domain, conducts its ciliary functions from PI3P-enriched EEs.

The RABS-5 ciliary pathway involves VPS-45 but may be independent of RAB-5

In the canonical model of EE formation and maturation, RAB5 first establishes a local PI3P-enriched endomembrane domain by recruiting and activating the phosphoinositide 3-kinase (PI3K) (Li *et al*, 1995; Christoforidis *et al*, 1999b; Somsel Rodman & Wandinger-Ness, 2000; Lawe *et al*, 2002; Mayinger, 2012; Fig 3A). Subsequently, RAB5 and PI3P cooperatively recruit FYVE domain-containing proteins involved in EE membrane tethering and fusion such as EEA1 and Rabenosyn-5 (Patki *et al*, 1997; Gaullier *et al*, 1998, 1999, 2000; Mills *et al*, 1998; Simonsen *et al*, 1998; Christoforidis *et al*, 1999a; McBride *et al*, 1999; Lawe *et al*, 2000; Abe *et al*, 2009). Rabenosyn-5 facilitates homotypic fusion of incoming endocytic vesicles by binding the SM protein VPS45, which in turn stabilises endosomal SNARE protein activity (Gengyo-Ando *et al*, 2007; Morrison *et al*, 2008; Rahajeng *et al*, 2010; Fig 3A). In addition to sorting proteins for lysosomal degradation, Rabenosyn-5 interacts with EHD1 to recycle proteins back to the plasma membrane, either directly or via the endocytic recycling compartment (Naslavsky *et al*, 2004; Navaroli *et al*, 2012; Fig 3A).

Since the Rab binding domain is not required for RABS-5 localisation and its regulation of cilium structure (Fig 2), we investigated whether RAB-5 functions upstream in the RABS-5 ciliary pathway. First, we asked whether RAB-5 activity regulates RABS-5 localisations by examining RFP::RABS-5 in worms overexpressing dominant constitutively active (Q78L; GTP bound) or inactive (S33N; GDP bound) variants of RAB-5 (Fig 3B). In both scenarios, RABS-5 retained a seemingly identical vesicle-like distribution in the cell bodies, despite a diffuse localisation for RAB-5(S33N) and an EE-like localisation for RAB-5(Q78L) (compare Fig 3B with Fig 2E). Thus, RABS-5 recruitment to EE-like structures occurs independently of the RAB-5 activation state. Next, we assessed whether RAB-5(Q78L) or RAB-5(S33N) overexpression, or loss of RAB-5 GEFs (*rme-6* or *rabx-5*) (Sato *et al*, 2005; Sann *et al*, 2012), phenocopy the cilium structure defects of *rabs-5* mutants. In all cases, no defects in

Figure 3. Loss of VPS-45 phenocopies the ciliary defects of worms lacking RABS-5.

A Schematic summarising current models of Rabenosyn-5 function in early endosome maturation and protein sorting via degradative and recycling pathways. (1) Following an endocytic event, RAB5 is targeted to and activated on endocytic vesicles by GEF proteins (RABX-5, RME-6 in *Caenorhabditis elegans*). (2) Activated RAB5 (GTP) recruits and activates the phosphoinositide 3-kinase (PI3K) leading to local enrichment of phosphatidylinositol (3)-phosphate (PI3P) and the establishment of the early endosome (EE). (3) FYVE domain-containing RAB5 effectors (EEA1, Rabenosyn-5) are recruited in a PI3P-dependent manner and control EE fate towards lysosomal degradation (via Rabenosyn-5 recruitment of VPS45 that drives SNARE protein-dependent homotypic fusion events, and early-to-late endosome (LE) conversion) or recycling towards the endocytic recycling compartment [via Rabenosyn-5 recruitment of EHD1 (orthologue of *C. elegans* RME-1), dephosphorylation of PI3P, RAB-5 inactivation and tethering to early recycling compartment (ERC)].

B Representative images (Z-projects) of WT worms expressing *arl-13*p::*rfp*::*rabs-5*(WT) and either *arl-13*p::*gfp*::*rabs-5(S33N)* or *arl-13*p::*gfp*::*rabs-5(Q78L)*. Cell body regions are shown in left-hand column; distal dendrite/cilia regions are shown in right-hand column. White arrowhead indicates colocalised RAB-5 and RABS-5 EE signals. Unfilled arrowhead indicates RABS-5 signals that are uncoupled from RAB-5 signals. PCMC, periciliary membrane compartment. Anterior is to the left. Scale bars = 5 μm.

C Quantification of DiI uptake in the phasmid neurons of the indicated genetic backgrounds. In each case, the number (0–4) of phasmid neurons taking up dye is scored. Bars show phenotype frequency (%) from four independent experiments ($n > 35$ per experiment). Constitutive activation of RAB-5(Q78L) does not rescue the *rabs-5* dye-filling phenotype. *ups-45(tm0246)* worms phenocopy the *rabs-5(ok1513)* dye-filling defect. The *ups-45(tm0246)* dye-filling defect is rescued by reintroduction of wild-type *ups-45* sequences under a ciliated cell-specific promoter (*arl-13*p). The *rabs-5(ok1513);ups-45(tm0246)* double-mutant dye-filling phenotype is the same as the corresponding single mutants.

D Representative images and quantification of phasmid length and PCMC area in WT and *ups-45(tm0246)* mutant worms expressing *xbx-1*::*tdTomato* (length) and *rpi-2*::*gfp* (PCMC area). Bars show mean ± SEM ($n = 60$). *$P < 0.001$ (unpaired Student's *t*-test; vs. WT). PCMC, periciliary membrane compartment. Anterior is to the left. Scale bars = 5 μm.

E VPS-45 colocalises similarly with RABS-5(WT) and RABS-5(ΔFYVE). Shown are representative images (Z-stack projects) of the phasmid neurons of worms expressing *arl-13*p::*ups-45*::*gfp* and either *arl-13*p::*rfp*::*rabs-5(WT)* or *arl-13*p::*rfp*::*rabs-5(ΔFYVE)*. Cell body regions are shown in left-hand columns; distal dendrite/cilia regions are shown in right-hand columns. Arrowheads indicate colocalised RABS-5 and VPS-45 early endosomes (EE). Top graph, quantification of VPS-45::GFP and RFP::RABS-5 EE colocalisation in the cell bodies. Bars show mean ± SEM from 11 to 13 independent experiments (total number of vesicles counted is indicated above each bar). Bottom graph, quantification of VPS-45 and RABS-5 PCMC signal enrichment. Black unfilled bars: worms co-expressing *ups-45*::*gfp* + *rfp*::*rabs-5(WT)*. Grey filled bars, worms co-expressing *ups-45*::*gfp* + *rfp*::*rabs-5(ΔFYVE)*. Bars show mean ± SEM values ($n = 27$–31 per condition). *$P < 0.001$ (unpaired Student's *t*-test). PCMC, periciliary membrane compartment. Anterior is to the left. Scale bars = 5 μm.

F VPS-45 localisation in *rabs-5* mutant. Representative images (Z-stack projects) of phasmid neurons in WT and *rabs-5(ok1513)* worms expressing *arl-13*p::*ups-45*::*gfp*. Graph shows VPS-45::GFP signal enrichment at early endosome (EE)-like structures (arrowheads). Bars show mean ± SEM values (total number of vesicles counted is indicated above each bar). *$P < 0.001$ (unpaired Student's *t*-test, vs. WT). PCMC, periciliary membrane compartment. Anterior is to the left. Scale bars = 5 μm.

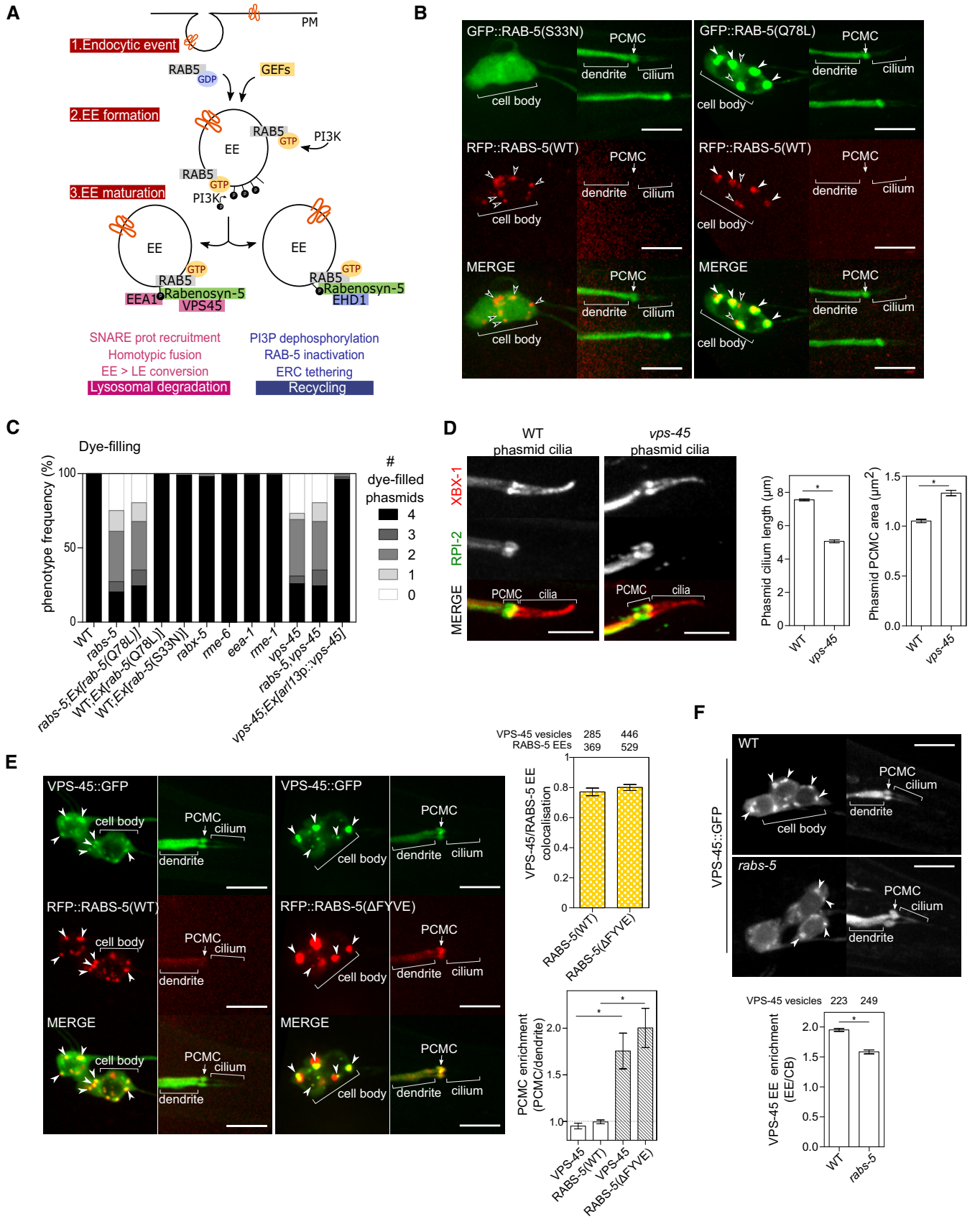
A
PM
1.Endocytic event
RAB5
GDP
GEFs
2.EE formation
EE
RAB5
GTP
PI3K
3.EE maturation
EEA1
VPS45
Rabenosyn-5
EHD1
SNARE prot recruitment
Homotypic fusion
EE > LE conversion
Lysosomal degradation
PI3P dephosphorylation
RAB-5 inactivation
ERC tethering
Recycling
B
GFP::RAB-5(S33N)
GFP::RAB-5(Q78L)
RFP::RABS-5(WT)
MERGE
PCMC
dendrite
cilium
cell body
C
Dye-filling
phenotype frequency (%)
dye-filled phasmids
WT
rabs-5
rabs-5;Ex[rab-5(Q78L)]
WT;Ex[rab-5(Q78L)]
WT;Ex[rab-5(S33N)]
rabx-5
rme-6
eea-1
rme-1
vps-45
rabs-5;vps-45
vps-45;Ex[arl13p::vps-45]
D
WT phasmid cilia
vps-45 phasmid cilia
XBX-1
RPI-2
MERGE
PCMC
cilia
Phasmid cilium length (µm)
Phasmid PCMC area (µm2)
E
VPS-45::GFP
RFP::RABS-5(WT)
RFP::RABS-5(ΔFYVE)
VPS-45 vesicles 285 446
RABS-5 EEs 369 529
VPS-45/RABS-5 EE colocalisation
PCMC enrichment (PCMC/dendrite)
F
WT
rabs-5
VPS-45 vesicles 223 249
VPS-45 EE enrichment (EE/CB)

Figure 3.

phasmid dye-filling, cilium length, or PCMC area were observed (Figs 3C and EV3A and B; Hu *et al*, 2007; Kaplan *et al*, 2012; van der Vaart *et al*, 2015). Similar observations were made for a mutant of the RAB-5 effector, *eea-1* (Figs 3C and EV3A). We also found that overexpression of activated RAB-5(Q78L) does not rescue (i.e. bypass) the dye-filling and PCMC defects of *rabs-5* mutants (Figs 3C and EV3B). Together, these data suggest that the *rabs-5* ciliary pathway does not involve RAB-5.

Analysis of known downstream effectors of RABS-5 revealed that a loss-of-function allele of *rme-1* (EHD1 orthologue) displays normal dye-filling, phasmid cilium length and PCMC area (Figs 3C and EV3A). In contrast, a loss-of-function allele (*tm0246*) that disrupts exons 1-4 of *vps-45* phenocopies the ciliary defects of the *rabs-5* mutant. Specifically, *vps-45* mutants are dye-filling defective (phasmids), possess short phasmid cilia, display enlarged PCMCs and exhibit a reduced roaming behaviour (Figs 3C and D, and EV3C–E). In additional similarity to *rabs-5*, the early stages of cilium formation are also regulated by *vps-45*, and *vps-45(tm0246)* ciliary defects are modestly exacerbated by higher growth temperature (Fig EV3C and E). Expression of wild-type *vps-45* genomic sequence under an *arl-13* promoter rescues the *vps-45* mutant dye-filling phenotype, indicating that VPS-45 functions in ciliated cells (Fig 3C). Indeed, a GFP reporter under the control of *vps-45* upstream regulatory sequences is expressed in ciliated cells, although not exclusively (Fig EV3F; Gengyo-Ando *et al*, 2007).

We also found that the *rabs-5;vps-45* double-mutant dye-filling defect is comparable to that of the corresponding single mutants, indicating that both genes function in the same cilia-related pathway (Fig 3C). Consistent with this notion, a VPS-45::GFP reporter colocalises with RFP::RABS-5-marked EEs in the cell bodies of ciliated neurons [Figs 3E and EV3G (whole neuron images)]. Moreover, RABS-5 is required for normal VPS-45 EE localisation in ciliated cells (Fig 3F), and overexpression of the mislocalised RABS-5(ΔFYVE) variant causes a similar mislocalisation and accumulation of VPS-45 to the PCMC and to ectopic RABS-5(ΔFYVE)-positive vesicles in the dendrites and cell bodies (Figs 3E and EV3G and H). Thus, RABS-5 is both necessary and sufficient for VPS-45 EE localisation in ciliated cells.

These findings show that RABS-5 and VPS-45 function together in ciliated cells to regulate ciliary membrane structure and function, and suggest that this pathway may not involve upstream RAB-5 functions.

RABS-5 and VPS-45 control the levels of a subset of PCMC-associated endocytic vesicles and regulators

To further investigate *rabs*-5 and *vps-45* regulation of ciliary and periciliary membrane homeostasis, we examined the ultrastructure of hermaphrodite and male-specific cilia using transmission electron microscopy (TEM). Consistent with a wild-type dye-filling phenotype in the head, we found that the amphid channel ciliary axonemes of *rabs-5* and *vps-45* mutants are mostly intact, with normal distal segment and middle segment subcompartments (Appendix Fig S1). However, although most transition zones (TZ) appear normal, there are rare examples of *rabs-5* and *vps-45* mutant TZs with > 9 singlet microtubules, which is never observed in WT controls (Appendix Fig S1). However, in agreement with our fluorescence data, most mutant cilia possess enlarged PCMCs, and the OLQ ciliary membrane is expanded (Fig 4A and Appendix Figs S1 and S2A). Strikingly, the *vps-45* and *rabs-5* mutant PCMCs of all examined ciliated cells (male and hermaphrodite), including amphid channel, labial and CEM neurons, possess large accumulations of small uncoated vesicles (~40.1 ± 0.4 nm diameter for *rabs-5*; 39 ± 0.5 nm diameter for *vps-45*; Fig 4A and Appendix Figs S1 and S2A and B). These vesicles frequently appear to accumulate in the distal regions of the PCMC, near the basal body region, suggesting a functional connection with the cilium (Appendix Fig S1). In addition, large extracellular vesicle-like structures strongly accumulate within the male CEM/CEP pore and occasionally in other pores (Appendix Fig S2A).

The accumulated PCMC vesicles in *rabs-5* and *vps-45* mutants indicate a defect in periciliary membrane endocytic regulation. To test this further, we examined the PCMC localisations of fluorescence reporters of various endocytic regulators, namely the AP-2 clathrin adapter (DPY-23::GFP), endosomes (RFP::EEA-1, GFP::RAB-5, WDFY-2::GFP) and caveolin (GFP::CAV-1). In wild-type worms, all reporters except EEA-1 localise at the PCMC (Figs 4B and EV4A). In addition, WDFY-2- and RAB-5-positive vesicles traffic along the dendrites (Fig EV4B; Hu *et al*, 2007; Kaplan *et al*, 2012; van der Vaart *et al*, 2015). WDFY-2 signals also colocalise with RABS-5-positive EEs in the cell bodies (Fig EV4C). Therefore, we confirm previously described PCMC localisations for AP-2 and RAB-5 and reveal new PCMC associations for caveolae-associated protein 1 (CAV-1), as well as the WD40 and FYVE domain-containing protein 2 (WDFY-2) that marks a subset of RAB-5-negative EEs (Hayakawa

Figure 4. RABS-5 and VPS-45 control PCMC vesicle number and the PCMC levels of a subset of endocytic regulators and ciliary membrane proteins.

A TEM images from thin sections showing PCMC ultrastructure of WT, *rabs-5(ok1513)* and *vps-45(tm0246)* amphid pores (hermaphrodite) (left) and male-specific CEM neurons (right). For amphid images, low-magnification images of the entire pore are shown in the left images; right-hand images show one representative PCMC at high magnification (Mag). Red outline denotes the PCMCs. Blue arrowheads denote uncoated vesicles. Green arrowheads denote coated vesicles. Yellow arrowheads denote extracellular vesicles in the amphid or cephalic pore. Schematics show the amphid and cephalic (CEP/CEM) channels, as well as the OLQ cilium, in longitudinal section. For simplicity, the cartoon of the amphid pore only shows 3 of the 10 cilia. Arrows in schematics indicate the relative position of the sections shown. Cartoons also show the PCMC phenotype of *rabs-5* and *vps-45* mutants. PCMC, periciliary membrane compartment.

B Representative images (Z-projects) of the head regions of hermaphrodite WT, *rabs-5(ok1513)* and *vps-45(tm0246)* worms expressing *arl-13*p::*gfp*::*cav-1* or *arl-13*p::*wdfy-2*::*gfp*. Images show the ciliary regions (left panels) and the cell bodies regions (right panels). Anterior is to the left. Scale bars = 5 μm.

C Quantification of PCMC signal enrichment and cell body vesicle number for the indicated markers (expressed in ciliated cells by *arl-13* promoter sequences) in ciliated neurons of WT and *rabs-5(ok1513)* worms. Bars show mean ± SEM (n = 20–30 per condition). *P < 0.01 (nonparametric Mann–Whitney U-test; vs. WT).

D Representative images (Z-projects) of male head and tail regions in WT, *rabs-5(ok1513)* and *vps-45(tm0246)* worms expressing *pkd-2*::*gfp*. PCMC, periciliary membrane compartment. Anterior is to the left. Scale bars = 5 and 2.5 μm (high magnification insets).

E Quantification of PCMC and ciliary axonemal relative mean intensities for *pkd-2*::*gfp* (expressed in male-specific neurons), *srbc-66*::*gfp* (expressed in ASK neurons) and *osm-9*::*gfp* (expressed in OLQ neurons of WT and *rabs-5(ok1513)* worms. Bars show mean ± SEM (n = 30). *P < 0.001 (unpaired Student's t-test, vs. WT).

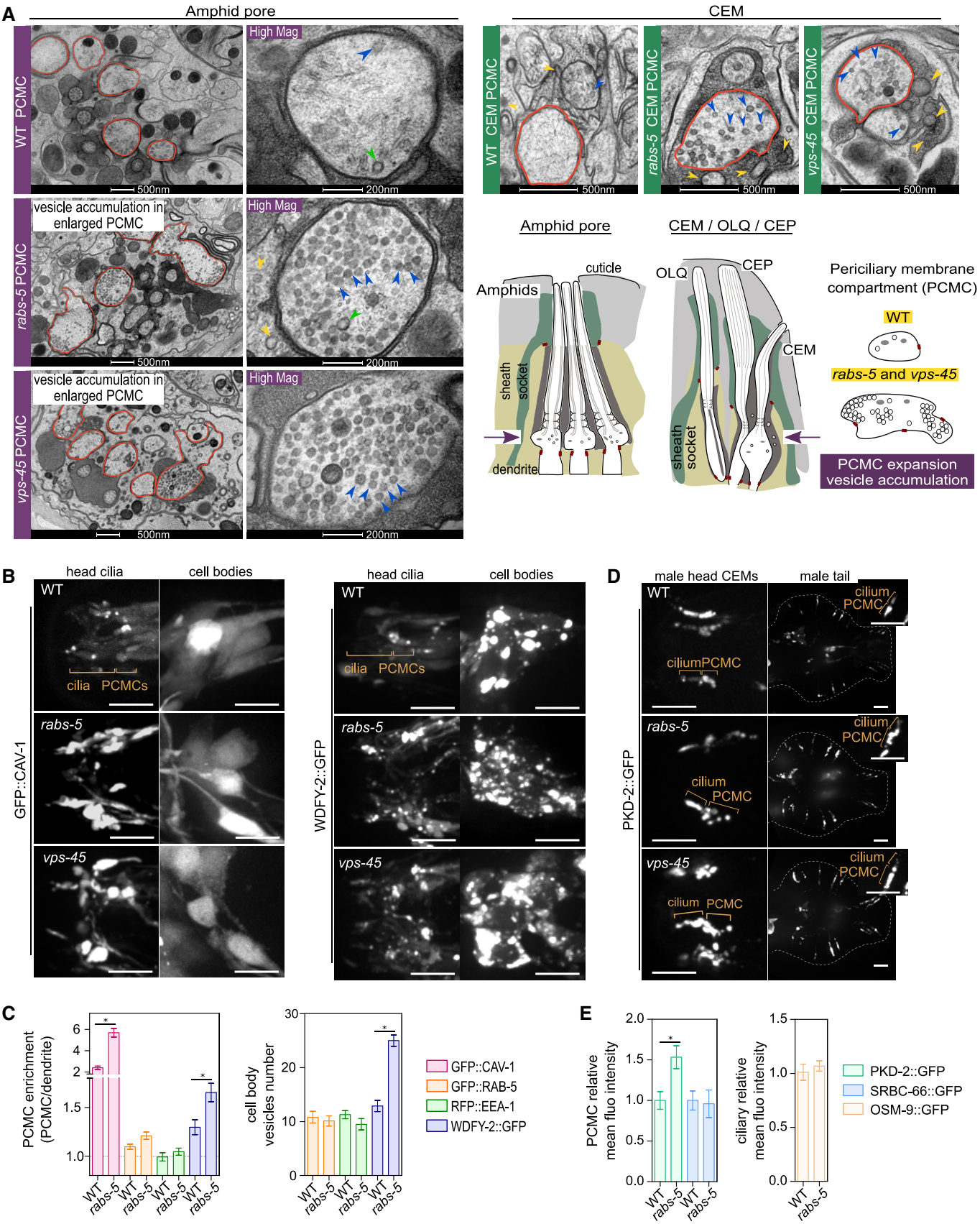

Figure 4.

et al, 2006). In *rabs-5* and *vps-45* mutant PCMCs, we observed a striking increase in CAV-1 levels, and a more modest increase in WDFY-2 levels, whereas DPY-23, RAB-5 and EEA-1 levels are unaltered (Figs 4B and C, and EV4A and B). We also found increased numbers of small WDFY-2-positive vesicles in the cell bodies of *rabs-5* and *vps-45* mutants, suggestive of unfused EEs (Fig 4B and C). Thus, RABS-5 and VPS-45 regulate the PCMC levels of a subset of endocytic regulators (WDFY-2, CAV-1).

Next, we wondered whether the accumulated endocytic vesicle phenotype in the PCMC correlates with a defect in ciliary protein localisation or distribution. Using various fluorescence reporters, we found that the polycystin-2 protein orthologue (PKD-2) expressed in males (Barr & Sternberg, 1999; Barr *et al*, 2001) accumulates in the PCMCs of *rabs-5* and *vps-45* mutant worms (Fig 4D and E). In contrast, loss of *rabs-5* function does not alter the ciliary localisations of OSM-9 (TRPV channel expressed in OLQ neuron; Colbert *et al*, 1997), STR-2 (olfactory receptor expressed in AWC neuron; Troemel *et al*, 1999) or SRBC-66 (GPCR expressed in ASK neuron; Kim *et al*, 2009; Figs 1F and EV4D). We conclude, therefore, that RABS-5 controls the localisation of a subset of ciliary proteins in specific neurons. Our data also suggest that the vesicles accumulating in the *rabs-5* and *vps-45* mutant PCMCs are cilia-related.

Integration of RABS-5, VPS-45 and CAV-1 cilia-related functions for PKD-2 homeostasis and male mating behaviour

Our data implicate functional links between RABS-5/VPS-45 regulation of CAV-1, a subset of EEs (WDFY-2-positive) and PKD-2 homeostasis. To better integrate our findings, we investigated these links further in PKD-2-expressing male-specific ciliated neurons.

First, we found enriched pools of RFP::CAV-1 and WDFY-2::RFP in the PCMCs of male CEM and ray tail neurons (Fig 5A, C and D). PKD-2 and WDFY-2 also colocalise on EEs that bidirectionally traffic along the dendrites between the cilium and the cell body; however, unlike PKD-2, WDFY-2 is excluded from cilia and ciliary ectosomes (Fig 5A and B, and Movie EV2). The PCMC levels of CAV-1 and WDFY-2 are also increased in the PCMCs of *rabs-5* males (Fig 5A, C and D). Thus, like in hermaphrodites, RABS-5 regulates CAV-1 and WDFY-2 PCMC levels in male-specific neurons.

Next, we found that PKD-2 levels are reduced in the PCMC of worms overexpressing RABS-5 (Fig 5E). This finding contrasts with the opposite phenotype (increased levels) for *rabs-5* mutant worms (Fig 5F) and is consistent with RABS-5 being a positive regulator of ciliary PKD-2 turnover. Strikingly, PKD-2::GFP levels are drastically reduced in the ciliary region of WT and *rabs-5* mutant worms overexpressing RFP::CAV-1 (Figs 5C and E, and EV5B). We also found that the ciliary and PCMC levels of PKD-2 are reduced in a loss-of-function mutant of *cav-1* (Fig 5F). Thus, unlike RABS-5, both overexpression and loss of CAV-1 cause a reduction in PKD-2 ciliary levels. In contrast, neither overexpression nor loss of WDFY-2 affected PKD-2 localisations (Fig 5A, E and F). Together, these data indicate that in addition to RABS-5 and VPS-45, PKD-2 ciliary homeostasis requires CAV-1, but not WDFY-2.

To further examine the relationships between *rabs-5*, *vps-45* and *cav-1* in regulating PKD-2 ciliary levels, we performed epistasis analyses. In *rabs-5*;*vps-45* double mutants, the PKD-2 localisation phenotype is identical to that of the single mutants (i.e. increased PCMC levels; Fig 5F), indicating that these genes serve closely linked functions in the same PKD-2 sorting pathway, similar to what we report above for their relationship in cilium structure regulation. In contrast, the *rabs-5*;*cav-1* double-mutant possesses the same PKD-2 accumulation (PCMC) phenotype as the *rabs-5* single mutant, demonstrating that *rabs-5* is epistatic to *cav-1* (Fig 5F). This finding indicates that *rabs-5* and *cav-1* function at distinct steps of common or intersecting pathways. Consistent with this notion, the regulation of CAV-1 levels at the PCMC is dependent on *rabs-5* but not vice versa (Figs 5D and EV5A).

Figure 5. Regulation of PKD-2 ciliary homeostasis and associated male mating behaviour via RABS-5, VPS-45 and CAV-1.

A Representative images (Z-projects) of the head (CEM cilia) and tail (ray neurons) regions of WT and *rabs-5(ok1513)* male worms co-expressing *pkd-2p::wdfy-2::rfp* and *pkd-2::gfp*. Inset in tail images shows a set of ray cilia at higher magnification. Arrowheads denote PKD-2::GFP in ectosomes released from the CEM pore. PCMC, periciliary membrane compartment. Anterior is to the top. Scale bars = 5 and 2.5 μm (insets).

B Representative time-lapse images and kymographs of the CEM dendritic regions of WT worms co-expressing *pkd-2p::wdfy-2::rfp* and *pkd-2::gfp*. Images correspond to frames from videos where GFP and RFP signals were simultaneously imaged. Arrowheads denote colocalised signals. Asterisks, non-moving foci as a reference. Anterior is to the left. s, seconds. Scale bars = 5 μm on time-lapse images. On kymograph, vertical scale indicates time (5 s); horizontal scale indicates distance (5 μm).

C Representative images (Z-projects) of head (CEM cilia) and tail (ray neurons) regions of WT and *rabs-5(ok1513)* male worms co-expressing *pkd-2p::rfp::cav-1* and *pkd-2::gfp*. Inset in tail images shows a set of ray cilia at higher magnification. PCMC, periciliary membrane compartment. Anterior is to the top. Scale bars = 5 and 2.5 μm (insets).

D Quantification of CAV-1 and WDFY-2 PCMC signal enrichment in the CEM neurons of WT and *rabs-5(ok1513)* worms expressing *pkd-2p::rfp::cav-1* or *pkd-2p::wdfy-2::rfp*. Bars show mean ± SEM (n = 25). *P < 0.01 (nonparametric Mann–Whitney U-test; vs. WT).

E Quantification of PKD-2::GFP levels at the PCMC of CEM neurons in WT and *rabs-5(ok1513)* mutants expressing *pkd-2p::rfp::cav-1*, *pkd-2p::rfp::rabs-5*, or *pkd-2p::wdfy-2::rfp*. Bars show mean ± SEM (n > 30). *P < 0.05; ***P < 0.0001 (nonparametric Mann–Whitney U-test).

F Representative images (Z-projects) and quantification of PKD-2::GFP enrichment CEM cilia PCMC of WT, *rabs-5(ok1513)*, *vps-45(tm0246)*, *wdfy-2(ok3592)* and *cav-1 (ok2089)* single mutants, and *rabs-5(ok1513);cav-1(ok2089)* and *rabs-5(ok1513);vps-45(tm246)* double mutants. Bars show mean ± SEM values (n < 40). *P < 0.001 (nonparametric Mann–Whitney U-test; vs. WT). ns, not significant. Scale bars = 5 μm.

G Quantification of male mating behaviours (response initiation and vulval location) for the indicated mutant strains [allele details in (F)]. Bars show mean ± SEM values from three independent experiments (n = 20 per experiment). *P < 0.001 (unpaired Student's t-test; vs. WT).

H Model of RABS-5/VPS-45 and CAV-1 control of PKD-2 homeostasis at the cilium and PCMC. PKD-2 sorting from the cilium is controlled via addition of post-translational modifications (ubiquitination/phosphorylation) acting as sorting signals (Hu *et al*, 2007). At the periciliary membrane, CAV-1-mediated endocytosis loads PKD-2 onto endocytic vesicles (1), which subsequently undergo RABS-5 and VPS-45-mediated fusion with EEs (2), followed by sorting for lysosomal degradation via ESCRT proteins (Hu *et al*, 2007), or recycling back to the periciliary membrane via the endocytic recycling compartment (ERC). Note that a subsidiary route may involve clathrin-mediated endocytosis (refer to Discussion section for details). EV, extracellular vesicles.

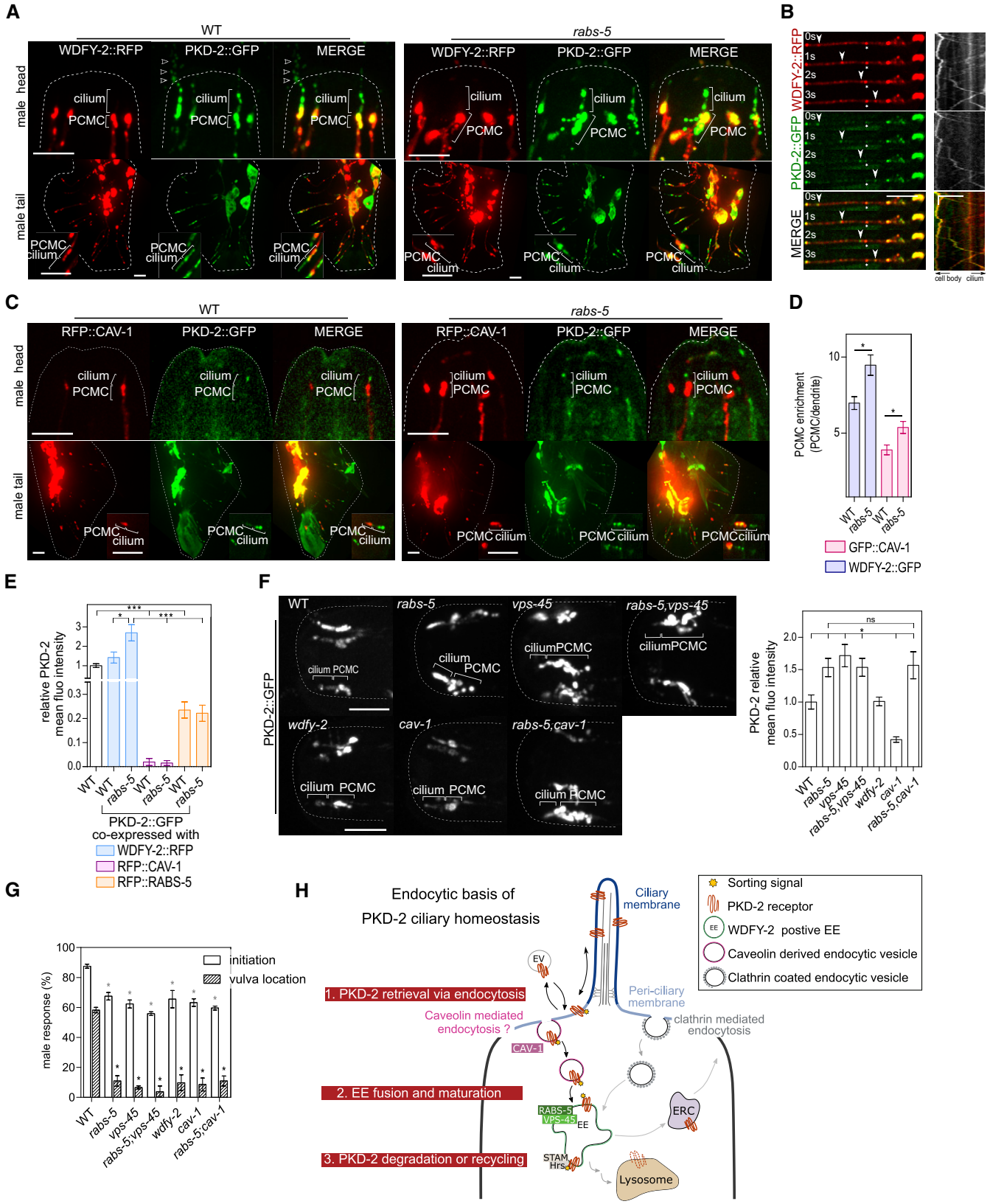
A
WT
rabs-5
WDFY-2::RFP
PKD-2::GFP
MERGE
male head
male tail
cilium
PCMC
B
WDFY-2::RFP
PKD-2::GFP
MERGE
0s
1s
2s
3s
cell body
cilium
C
RFP::CAV-1
D
PCMC enrichment (PCMC/dendrite)
GFP::CAV-1
WDFY-2::GFP
E
relative PKD-2 mean fluo intensity
PKD-2::GFP co-expressed with
WDFY-2::RFP
RFP::CAV-1
RFP::RABS-5
F
PKD-2::GFP
wdfy-2
cav-1
rabs-5,cav-1
rabs-5,vps-45
vps-45
ciliumPCMC
PKD-2 relative mean fluo intensity
ns
G
male response (%)
initiation
vulva location
H
Endocytic basis of
PKD-2 ciliary homeostasis
Ciliary membrane
Peri-ciliary membrane
EV
1. PKD-2 retrieval via endocytosis
Caveolin mediated endocytosis ?
CAV-1
clathrin mediated endocytosis
2. EE fusion and maturation
RABS-5
VPS-45
EE
ERC
3. PKD-2 degradation or recycling
STAM
Hrs
Lysosome
Sorting signal
PKD-2 receptor
WDFY-2 postive EE
Caveolin derived endocytic vesicle
Clathrin coated endocytic vesicle

Figure 5.

Finally, we wondered whether altered regulation of PKD-2 homeostasis in *rabs-5*, *vps-45* and *cav-1* mutants disrupts male mating behaviour. In all cases, mutant males display a reduced male mating engagement response to wild-type hermaphrodites and a reduced ability to locate the hermaphrodite vulva (Fig 5G). Male mating behaviour defects were also observed for *wdfy-2* mutants, despite normal PKD-2 localisations in these worms (Fig 5G).

Together, these data establish functional associations between *cav-1*, *rabs-5/vps-45* and *wdfy-2* in the endocytic control of PKD-2 ciliary levels and/or associated function.

Discussion

By employing a reverse genetics approach in *C. elegans*, we have identified essentially identical ciliogenic and PKD-2 turnover roles for RABS-5 (Rabenosyn-5) and VPS-45 (VPS45), which form an interacting pair that control EE homotypic fusion and protein sorting in other subcellular contexts (Nielsen *et al*, 2000; Gengyo-Ando *et al*, 2007; Morrison *et al*, 2008). Specifically, we show that loss of RABS-5 or VPS-45 causes: (i) expanded ciliary and periciliary membranes, (ii) PCMC accumulation of uncoated vesicles, (iii) increased cell body and/or PCMC levels of select endocytic regulators and EE markers (CAV-1, WDFY-2), (iv) increased PCMC levels of select ciliary receptors (PKD-2) and (v) disrupted cilium-associated sensory functions (male mating and roaming behaviours). In further support of roles in the same cilia-related pathway, *rabs-5; vps-45* double mutants phenocopy the ciliogenic and PKD-2 homeostasis phenotypes of the single mutants, both proteins colocalise on EEs, and RABS-5 is necessary and sufficient for VPS-45 localisation in ciliated cells. As additional evidence that RABS-5 positively regulates ciliary protein sorting and turnover, RABS-5 overexpression reduces the PCMC levels of PKD-2. Together, these data indicate that RABS-5 and VPS-45 are not global ciliogenic factors, but rather they facilitate ciliary and periciliary membrane structure and function by regulating specific PCMC-derived endocytic vesicles (CAV-1, WDFY-2) and ciliary cargo (PKD-2). Our findings also suggest that RABS-5 and VPS45 serve specific functions in male-specific ciliated sensory neurons that release extracellular vesicles. Thus, our study describes new ciliary roles for Rabenosyn-5 and VPS45, and provides insight into endocytic regulation of ciliary membrane homeostasis.

We propose that the ciliary phenotype in *rabs-5* and *vps-45* mutants relates to a specific defect in EE homotypic fusion. This conclusion is based on a number of key observations. First, TEM analysis revealed abnormally large numbers of vesicles in the PCMCs of *rabs-5* and *vps-45* mutants. Second, these mutants possess increased numbers of small fluorescently labelled WDFY-2-marked EEs in the cell bodies. Third, the dominant-negative RABS-5 (ΔFYVE) variant associates with abnormally large vesicles, consistent with aberrant membrane fusion. These observations are consistent with EE fusion and maturation defects associated with Rabenosyn-5, VPS45 and RAB5 in other contexts, including *C. elegans* macrophage-like cells, *Drosophila* and mammalian cell culture (Nielsen *et al*, 2000; Gengyo-Ando *et al*, 2007; Morrison *et al*, 2008).

Analysis of RABS-5 subcellular localisations indicates common and distinct sites of action in ciliated neuronal cell types. In the majority of analysed cells, functional RABS-5 and VPS-45 is found at EEs in the cell bodies, with no enrichment at the ciliary base region. This polarised distribution implies that endocytic vesicles derived from the cilium must first be transported to the cell body prior to maturation via RABS-5 and VPS-45 activities. Consistent with such an upstream delivery step, we and others have found that vesicles positive for EE markers (WDFY-2, RAB-5) and ciliary receptor cargos (e.g. PKD-2, ODR-10) traffic along the dendrites, between the PCMCs and cell bodies (Kaplan *et al*, 2012). In a subset of male-specific ciliated neurons, however, an enriched pool of RABS-5 occurs at the ciliary base region, indicating that the PCMC represents an additional site of RABS-5 and VPS-45 endosomal function in these cells. In support of this notion, EE-associated STAM-1 and Hrs proteins involved in PKD-2 sorting and lysosomal degradation also localise at the ciliary base of male-specific cells (Hu *et al*, 2007). Although the reason for this cell type-specific distribution is unclear, it may be that male-specific cilia require additional and more dynamic PCMC regulation of endocytosis because of their role in bioactive ectosome release and reception (Wood *et al*, 2013; Wang *et al*, 2014; Wang & Barr, 2016). Thus, cell type-specific endocytosis-related events such as the deployment of RABS-5 and VPS-45 at the PCMC may be a mechanism by which cilia are functionally diversified.

We found that RABS-5 and VPS-45 regulate the PCMC localisations of CAV-1 (caveolin-1 orthologue) and WDFY-2, but not the clathrin adaptor AP-2, RAB-5 or EEA-1. Thus, RABS- and VPS-45 control the PCMC levels of a specific set of endocytic regulators. Together with the observation that PKD-2 accumulates in the PCMC of *rabs-5* and *vps-45* mutants, we propose that at least some of the accumulated vesicles (observed by TEM) in the PCMC of these mutants are CAV-1- and/or WDFY-2-derived ciliary vesicles. Caveolin proteins, of which there are three in mammals (two in worms), form the coat scaffold of endocytic plasma membrane invagination called caveolae; caveolin-1 is functionally linked to cholesterol and membrane trafficking, as well as signal transduction (Hansen & Nichols, 2009; Kumari *et al*, 2010; Parton & del Pozo, 2013). WDFY-2 is a WD40 and FYVE domain-containing protein defining a subset of RAB-5- and EEA-1-negative EEs that function in the early steps of endocytosis (Hayakawa *et al*, 2006). To our knowledge, our study is the first to indicate WDFY-2-positive EEs at the ciliary region, and the PCMC enrichment of CAV-1 agrees with the ciliary base localisation for the mammalian orthologue in cultured cells (Schou *et al*, 2017). However, whether CAV-1 and WDFY-2 associate with PCMC vesicles will require further investigation using techniques such as immuno-EM.

Strikingly, we found that CAV-1 loss or overexpression reduces the PCMC levels of PKD-2 and abrogates male mating behaviour. Thus, like RABS-5 and VPS-45, the regulation of PKD-2 ciliary levels and associated function is CAV-1 dependent. We propose a model whereby PKD-2 homeostasis is controlled by CAV-1-regulated endocytosis from the periciliary membrane, followed by RABS-5- and VPS-45-dependent fusion and sorting events at the EE leading to lysosomal degradation or recycling (Fig 5H). However, a sole linear model involving CAV-1 and RABS-5/VPS-45 is challenged by our epistasis data that suggest a more complex mechanism of PKD-2 homeostatic regulation, involving additional compensatory pathways. Firstly, the PCMC accumulation of PKD-2 in *rabs-5* mutants does not require CAV-1 (Fig 5F), indicating the existence of

alternative PKD-2 endocytic uptake mechanisms. Although clathrin-mediated endocytosis is an attractive candidate, previous work found that PKD-2 ciliary levels are not affected in AP-2-disrupted worms (Bae *et al*, 2006). Secondly, the removal of PKD-2 from the cilium and PCMC via CAV-1 overexpression does not require RABS-5 (Fig 5C and E). Thus, whilst our *rabs-5* mutant data clearly demonstrate the role of RABS-5 in the PCMC turnover of PKD-2, an alternative route to PKD-2 clearance must exist in CAV-1-overexpressing cells. This route may involve the previously described endosome-associated STAM/Hrs proteins that sort phosphorylated and ubiquitinated PKD-2 for PCMC removal via lysosomal degradation (Hu *et al*, 2007); indeed, the observation that caveolin-1 overexpression increases ubiquitination machinery activity supports this notion (Hayer *et al*, 2010). Together, these data suggest that whilst PKD-2 homeostatic regulation at the cilium may involve a linear relationship between CAV-1-regulated retrieval and RABS-5/VPS-45, additional redundant pathways that separately employ CAV-1 and RABS-5/VPS-45 are also likely involved (Fig 5H). Whilst we describe a role for CAV-1 in regulating PKD-2 ciliary levels, it remains to be determined whether this function is mediated by caveolin-dependent endocytic events, especially since the role for caveolins in endocytosis is controversial in other contexts (Parton & del Pozo, 2013). Thus, further research will be required to investigate the caveolin-mediated endocytic pathway in relation to ciliary membrane homeostasis and associated signalling.

Somewhat surprisingly, we uncovered evidence that the RABS-5 and VPS-45 ciliogenic pathway may not depend on upstream RAB-5 regulation, despite Rabenosyn-5 being an effector of RAB5 in other contexts (Nielsen *et al*, 2000; Gengyo-Ando *et al*, 2007). Specifically, we observed that mutants of various RAB-5 GEFs (RME-6, RABX-5), or overexpression of dominant loss- or gain-of-function RAB-5 variants (GDP or GTP-locked), do not phenocopy the cilium structure phenotypes of *rabs-5* or *vps-45* mutants. Furthermore, we found that RABS-5 subcellular localisation in ciliated cells is not overtly affected by RAB-5(GDP) or RAB-5(GTP) overexpression, nor does constitutive activation of RAB-5 alter the ciliary phenotypes of *rabs-5* mutants. Although we were unable to assess the ciliary phenotype in RAB-5-null cells due to the requirement of the GTPase for viability, our findings suggest that the RABS-5/VPS-45 ciliogenic pathway is at least partially RAB-5-independent.

Finally, it is interesting to note that membrane trafficking genes such as RAB-5 and those related to clathrin-mediated endocytosis are largely dispensable for ciliogenesis whilst still participating in ciliary protein trafficking (reviewed in Blacque *et al*, 2018). Indeed, further analysis of two mutants from our original screen, *cav-1* and *wdfy-2*, confirms non-essential roles for these genes in defining cilium formation and morphology (Fig EV5C), yet both are required for ciliary PKD-2 homeostatic control (*cav-1*) and/or PKD-2-associated male mating behaviours (*cav-1*, *wdfy-2*). Thus, we cannot rule out the possibility that there are other genes in our screened list of 44, or in previous screens (Kaplan *et al*, 2010), that regulate ciliary membrane homeostasis events unrelated to ciliogenesis pathways. Future assessment of candidate membrane trafficking genes will need to take into account specific cilia-related transport pathways and functions.

In summary, this work describes new ciliary functions for EE regulators RABS-5 and VPS-45 and provides evidence of cilium-associated roles for caveolin-1 in *C. elegans*. Our findings also reveal insight into the endocytic regulation of PKD-2 levels and turnover at the cilium. Our study therefore reveals new perspectives for understanding the mechanisms underpinning ciliary membrane homeostasis regulation.

Materials and Methods

Caenorhabditis elegans strains and genetic crossing

Caenorhabditis elegans strains were maintained and cultured at 20°C (or 15°C for *rabs-5(ok1513)* and *vps-45(tm0246)*) using standard techniques (Brenner, 1974). All strains employed are shown in Appendix Table S2. Standard genetic crossing techniques were used to make double mutants and introduce transgenes into genetic backgrounds. Genotyping was performed using PCR (primer sequences in Appendix Table S3). All assays involving *rabs-5(ok1513)* and *vps-45(tm0246)* were performed with worms grown at 15°C unless otherwise indicated.

Fluorescence protein-tagged constructs and transgene generation

Constructs were generated by fusion PCR as previously described (Hobert, 2002). For the transcriptional GFP constructs, 5′ upstream sequences containing the promoter (including the first 11–19 bp of exon 1) for *rabs-5* (1,566 bp) and *vps-45* (1,075 bp) were amplified and fused to GFP amplified from pPD95.67. The *rabs-5* translational GFP fusion construct was generated by in-frame fusion of a GFP fragment (from pPD95.77) to a *rabs-5* genomic fragment consisting of the entire intronic and exonic sequence. For the C-terminal-tagged *vps-45, wdfy-2, dpy-23, str-2* and *jbts-14* fluorescent reporters expressed in ciliated cells, the entire intronic and exonic sequences of these genes were first fused to GFP or RFP sequences amplified from pPD95.77 and PCM10, respectively, followed by fusion of the resultant products to the 5′ upstream sequences of *arl-13* (214 bp), *pkd-2* (1,340 bp) or *str-2* (3,792 bp). For the N-terminal-tagged *rabs-5, rab-5, eea-1* and *cav-1* fluorescent reporters expressed in ciliated cells, the entire intronic and exonic sequences of these genes were fused to fragments consisting of the 5′ upstream sequences of *arl-13* (214 bp) or *pkd-2* (1,340 bp) already fused to GFP or RFP sequences. For the *rabs-5(ΔZnF)* (deletion of amino acids 23–44), *rabs-5(ΔFYVE)* (deletion of amino acids 170–230) and *rabs-5(ΔRBD)* (deletion of amino acids 517–557) fluorescent reporters (N-terminal-tagged), the entire intronic and exonic sequences that flank the region to be deleted were first fused in frame. The resultant products were then fused to a DNA fragment consisting of the 5′ upstream sequences of *arl-13* (214 bp) already fused to RFP sequence. To generate transgenic animals harbouring extrachromosomal arrays, all constructs were injected into N2 worms at 2.5 ng/μl (translational GFP constructs) or 50 ng/μl (transcriptional GFP constructs), together with a coelomycete cell-expressed co-injection marker (*unc-122*p::*gfp* or *unc-122*p::*dsRed*) injected at 100 ng/μl.

Dye-filling and behavioural assays

For the dye-filling assay, worms were incubated for 30 min in DiI (Invitrogen) solution (1/200 dilution in M9) and then recovered

on seeded NGM plates for 30 min (Sanders *et al*, 2015). Worms were subsequently mounted on slides, and DiI uptake into the ciliated amphid and phasmid cells was assessed using epifluorescence wide-field imaging. For the roaming (foraging) assay, single worms were placed for 18 h onto 55-mm seeded NGM plates and track coverage assessed using a grid reference to calculate roaming score (Sanders *et al*, 2015). For the osmotic avoidance assay, five worms were placed within a ring of 8 M glycerol (Sigma) supplemented with bromophenol blue (Alfa Aesar) on unseeded NGM plates and behaviour observed for 10 min. Worms crossing the barrier were removed from the assay (Sanders *et al*, 2015). The male mating behaviour assay was carried out as described previously (Peden & Barr, 2005; Bae *et al*, 2009). Briefly, staged L4 males were isolated 24 h before the assay. The following day, individual young adult males were placed with 15 hermaphrodites on a spot of food and observed for 4 min. The male response efficiency was determined by the fraction of males that initiated a contact response behaviour when encountering a hermaphrodite. For those males that initially responded to a hermaphrodite, the efficiency of vulva location was determined as the fraction of males locating the vulva within the duration of the assay.

Transmission electron microscopy

A total of 10–12 young adults worms were picked onto phosphatidylcholine-coated HPF (high-pressure freezer) carriers, packed with *Escherichia coli*. The carriers were frozen using the Leica EMPACT 2 HPF machine. Freeze substitution was performed in FS cocktail (1% OsO_4, 0.1% UA, 5% H20 in acetone; Cohen *et al*, 2008) in a solid metal block held at −80°C for two nights, followed by −20°C for one night, subsequent gradual temperature increase to four degrees, and finally incubation at room temperature for 1 h. Pellets were washed in acetone (3 × 1 h) and propylene oxide (3 × 1 h), followed by a 2-h incubation in 50:50 Epon:PO, then overnight incubation in a 70:30 EPON:PO solution and finally a 2-h room temperature incubation in 100% EPON. The worm pellet was emptied onto a Teflon-coated glass slide and gently teased apart with acupuncture needles. Individual worms were embedded in an EPON sandwich as described previously (Sanders *et al*, 2015). For male samples, virgin young L4 males were isolated and grown separately for 20 h before fixation.

Caenorhabditis elegans live fluorescent imaging

Fluorescence microscopy was conducted as described previously (Sanders *et al*, 2015). Staged young adult worms were mounted on 4% or 10% agarose pads. For PKD-2::GFP imaging, L4 males were isolated the day prior to recording. Epifluorescence images were taken on an upright Leica DM5000B and confocal images on an inverted Nikon Eclipse Ti microscope with a Yokogawa spinning-disc unit (Andor Revolution). Images were acquired using a charge-coupled device camera (iXon+EM-CCD, Andor Technology) and analysed using ImageJ software (Schneider *et al*, 2012). For dendritic transport, time-lapse movies of vesicles trafficking along the dendrite were recorded at 3.3 fps. Separated anterograde and retrograde kymographs were generated from multi-TIFF files using ImageJ plug-ins KymographClear (Mangeol *et al*, 2016).

Image analysis, quantification and statistical analysis

Axoneme length, PCMC and AWB fan area measurement were obtained from max projections of confocal Z-stacks generated using ImageJ software (Schneider *et al*, 2012). The PCMC enrichment of fluorescent protein-tagged reporters was calculated from Z-stack max projections as: (mean PCMC signal)/(mean distal dendrite end signal). For the RFP::RABS-5 constructs, the PCMC and distal dendrite end regions were defined by the GFP::RAB-5 signals. The enrichment of VPS-45::GFP signals on vesicles was calculated from Z-stack max projections as: (mean fluorescence of vesicle signal)/(mean fluorescence of neighbouring cytoplasm). Colocalisation of fluorescent vesicle-like structures was calculated from single-plane confocal images as: (number of vesicles displaying double labelling/total number of vesicles showing labelling of interest). Significance values calculated using a two-tailed Student's *t*-test or a nonparametric Mann–Whitney *U*-test as indicated in the figure legends were determined using GraphPad Prism software (www.graphpad.com).

Expanded View for this article is available online.

Acknowledgements
We thank the *Caenorhabditis* Genetics Center for strains. We thank laboratory members for comments and discussion of the manuscript. We are grateful to Dimitri Scholz and Tiina O'Neill of the UCD Conway Institute imaging facility for microscopy assistance. We also acknowledge Robert Crickley for the initial observation of a dye-filling defect in the *rabs-5* mutant. This work is funded by a Science Foundation Ireland Principal investigator award to OEB (11/PI/1037).

Author contributions
NS and OEB designed the study and co-wrote the manuscript. NS performed all experiments except the TEM, which was performed by JK.

Conflict of interest
The authors declare that they have no conflict of interest.

References

Abe M, Setoguchi Y, Tanaka T, Awano W, Takahashi K, Ueda R, Nakamura A, Goto S (2009) Membrane protein location-dependent regulation by PI3K (III) and rabenosyn-5 in *Drosophila* wing cells. *PLoS One* 4: e7306

Allen MA, Hillier LW, Waterston RH, Blumenthal T (2011) A global analysis of *C. elegans* trans-splicing. *Genome Res* 21: 255 – 264

Bae Y-K, Qin H, Knobel KM, Hu J, Rosenbaum JL, Barr MM (2006) General and cell-type specific mechanisms target TRPP2/PKD-2 to cilia. *Development* 133: 3859 – 3870

Bae Y-K, Kim E, L'Hernault SW, Barr MM (2009) The CIL-1 PI 5-phosphatase localizes TRP polycystins to cilia and activates sperm in *C. elegans*. *Curr Biol* 19: 1599 – 1607

Barr MM, Sternberg PW (1999) A polycystic kidney-disease gene homologue required for male mating behaviour in *C. elegans*. *Nature* 401: 386 – 389

Barr MM, DeModena J, Braun D, Nguyen CQ, Hall DH, Sternberg PW (2001) The *Caenorhabditis elegans* autosomal dominant polycystic kidney disease gene homologs lov-1 and pkd-2 act in the same pathway. *Curr Biol* 11: 1341 – 1346

Benmerah A (2013) The ciliary pocket. *Curr Opin Cell Biol* 25: 78 – 84

Blacque OE, Perens EA, Boroevich KA, Inglis PN, Li C, Warner A, Khattra J, Holt RA, Ou G, Mah AK, McKay SJ, Huang P, Swoboda P, Jones SJM, Marra MA, Baillie DL, Moerman DG, Shaham S, Leroux MR (2005) Functional genomics of the cilium, a sensory organelle. *Curr Biol* 15: 935 – 941

Blacque OE, Scheidel NE, Kuhns S (2018) Rab GTPases in cilium formation and function. *Small GTPases* 9: 76 – 94

Brenner S (1974) The genetics of *Caenorhabditis elegans*. *Genetics* 77: 71 – 94

Cao M, Ning J, Hernandez-Lara CI, Belzile O, Wang Q, Dutcher SK, Liu Y, Snell WJ (2015) Uni-directional ciliary membrane protein trafficking by a cytoplasmic retrograde IFT motor and ciliary ectosome shedding. *Elife* 4: e05242

Cevik S, Hori Y, Kaplan OI, Kida K, Toivenon T, Foley-Fisher C, Cottell D, Katada T, Kontani K, Blacque OE (2010) Joubert syndrome Arl13b functions at ciliary membranes and stabilizes protein transport in *Caenorhabditis elegans*. *J Cell Biol* 188: 953 – 969

Cevik S, Sanders AAWM, Van Wijk E, Boldt K, Clarke L, van Reeuwijk J, Hori Y, Horn N, Hetterschijt L, Wdowicz A, Mullins A, Kida K, Kaplan OI, van Beersum SEC, Man WuK, Letteboer SJF, Mans DA, Katada T, Kontani K, Ueffing M *et al* (2013) Active transport and diffusion barriers restrict Joubert Syndrome-associated ARL13B/ARL-13 to an Inv-like ciliary membrane subdomain. *PLoS Genet* 9: e1003977

Chávez M, Ena S, Van Sande J, de Kerchove d'Exaerde A, Schurmans S, Schiffmann SN (2015) Modulation of ciliary phosphoinositide content regulates trafficking and sonic hedgehog signaling output. *Dev Cell* 34: 338 – 350

Christoforidis S, McBride HM, Burgoyne RD, Zerial M (1999a) The Rab5 effector EEA1 is a core component of endosome docking. *Nature* 397: 621 – 625

Christoforidis S, Miaczynska M, Ashman K, Wilm M, Zhao L, Yip SC, Waterfield MD, Backer JM, Zerial M (1999b) Phosphatidylinositol-3-OH kinases are Rab5 effectors. *Nat Cell Biol* 1: 249 – 252

Clement CA, Ajbro KD, Koefoed K, Vestergaard ML, Veland IR, Henriques de Jesus MPR, Pedersen LB, Benmerah A, Andersen CY, Larsen LA, Christensen ST (2013) TGF-β signaling is associated with endocytosis at the pocket region of the primary cilium. *Cell Rep* 3: 1806 – 1814

Cohen M, Santarella R, Wiesel N, Mattaj I, Gruenbaum Y (2008) Chapter 21 electron microscopy of lamin and the nuclear lamina in *Caenorhabditis elegans*. *Methods Cell Biol* 88: 411 – 429.

Colbert HA, Smith TL, Bargmann CI (1997) OSM-9, a novel protein with structural similarity to channels, is required for olfaction, mechanosensation, and olfactory adaptation in *Caenorhabditis elegans*. *J Neurosci* 17: 8259 – 8269

Corbit KC, Aanstad P, Singla V, Norman AR, Stainier DYR, Reiter JF (2005) Vertebrate smoothened functions at the primary cilium. *Nature* 437: 1018 – 1021

Deretic D, Huber LA, Ransom N, Mancini M, Simons K, Papermaster DS (1995) rab8 in retinal photoreceptors may participate in rhodopsin transport and in rod outer segment disk morphogenesis. *J Cell Sci* 108 (Pt 1): 215 – 224

Deretic D (2013) Crosstalk of Arf and Rab GTPases en route to cilia. *Small GTPases* 4: 70 – 77

Dyson JM, Conduit SE, Feeney SJ, Hakim S, DiTommaso T, Fulcher AJ, Sriratana A, Ramm G, Horan KA, Gurung R, Wicking C, Smyth I, Mitchell CA (2017) INPP5E regulates phosphoinositide-dependent cilia transition zone function. *J Cell Biol* 216: 247 – 263

Eathiraj S, Pan X, Ritacco C, Lambright DG (2005) Structural basis of family-wide Rab GTPase recognition by rabenosyn-5. *Nature* 436: 415 – 419

Field MC, Carrington M (2009) The trypanosome flagellar pocket. *Nat Rev Microbiol* 7: 775 – 786

Fujiwara M, Sengupta P, McIntire SL (2002) Regulation of body size and behavioral state of *C. elegans* by sensory perception and the EGL-4 cGMP-dependent protein kinase. *Neuron* 36: 1091 – 1102

Garcia-Gonzalo FR, Phua SC, Roberson EC, Garcia G III, Abedin M, Schurmans S, Inoue T, Reiter JF (2015) Phosphoinositides regulate ciliary protein trafficking to modulate hedgehog signaling. *Dev Cell* 34: 400 – 409

Gaullier JM, Simonsen A, D'Arrigo A, Bremnes B, Stenmark H, Aasland R (1998) FYVE fingers bind PtdIns(3)P. *Nature* 394: 432 – 433

Gaullier JM, Simonsen A, D'Arrigo A, Bremnes B, Stenmark H (1999) FYVE finger proteins as effectors of phosphatidylinositol 3-phosphate. *Chem Phys Lipids* 98: 87 – 94

Gaullier J-M, Rønning E, Gillooly DJ, Stenmark H (2000) Interaction of the EEA1 FYVE finger with phosphatidylinositol 3-phosphate and early endosomes. *J Biol Chem* 275: 24595 – 24600

Gengyo-Ando K, Kuroyanagi H, Kobayashi T, Murate M, Fujimoto K, Okabe S, Mitani S (2007) The SM protein VPS-45 is required for RAB-5-dependent endocytic transport in *Caenorhabditis elegans*. *EMBO Rep* 8: 152 – 157

Goetz SC, Anderson KV (2010) The primary cilium: a signalling centre during vertebrate development. *Nat Rev Genet* 11: 331 – 344

Hansen CG, Nichols BJ (2009) Molecular mechanisms of clathrin-independent endocytosis. *J Cell Sci* 122: 1713 – 1721

Hayakawa A, Leonard D, Murphy S, Hayes S, Soto M, Fogarty K, Standley C, Bellve K, Lambright D, Mello C, Corvera S (2006) The WD40 and FYVE domain containing protein 2 defines a class of early endosomes necessary for endocytosis. *Proc Natl Acad Sci USA* 103: 11928 – 11933

Hayer A, Stoeber M, Ritz D, Engel S, Meyer HH, Helenius A (2010) Caveolin-1 is ubiquitinated and targeted to intralumenal vesicles in endolysosomes for degradation. *J Cell Biol* 191: 615 – 629

Hilgendorf KI, Johnson CT, Jackson PK (2016) The primary cilium as a cellular receiver: organizing ciliary GPCR signaling. *Curr Opin Cell Biol* 39: 84 – 92

Hobert O (2002) PCR fusion-based approach to create reporter gene constructs for expression analysis in transgenic *C. elegans*. *Biotechniques* 32: 728 – 730

Hu J, Wittekind SG, Barr MM (2007) STAM and Hrs down-regulate ciliary TRP receptors. *Mol Biol Cell* 18: 3277 – 3289

Hunnicutt GR (1990) Cell body and flagellar agglutinins in *Chlamydomonas reinhardtii*: the cell body plasma membrane is a reservoir for agglutinins whose migration to the flagella is regulated by a functional barrier. *J Cell Biol* 111: 1605 – 1616

Ismail S (2016) A GDI/GDF-like system for sorting and shuttling ciliary proteins. *Small GTPases* 8: 208 – 211

Jacoby M, Cox JJ, Gayral S, Hampshire DJ, Ayub M, Blockmans M, Pernot E, Kisseleva MV, Compère P, Schiffmann SN, Gergely F, Riley JH, Pérez-Morga D, Woods CG, Schurmans S (2009) INPP5E mutations cause primary cilium signaling defects, ciliary instability and ciliopathies in human and mouse. *Nat Genet* 41: 1027 – 1031

Jensen VL, Leroux MR (2017) Gates for soluble and membrane proteins, and two trafficking systems (IFT and LIFT), establish a dynamic ciliary signaling compartment. *Curr Opin Cell Biol* 47: 83 – 91

Kaplan OI, Molla-Herman A, Cevik S, Ghossoub R, Kida K, Kimura Y, Jenkins P, Martens JR, Setou M, Benmerah A, Blacque OE (2010) The AP-1 clathrin adaptor facilitates cilium formation and functions with RAB-8 in *C. elegans* ciliary membrane transport. *J Cell Sci* 123: 3966 – 3977

Kaplan OI, Doroquez DB, Cevik S, Bowie RV, Clarke L, Sanders AAWM, Kida K, Rappoport JZ, Sengupta P, Blacque OE (2012) Endocytosis genes facilitate

protein and membrane transport in *C. elegans* sensory cilia. *Curr Biol* 22: 451 – 460

Kathem SH, Mohieldin AM, Nauli SM (2014) The roles of primary cilia in polycystic kidney disease. *AIMS Mol Sci* 1: 27 – 46

Kim K, Sato K, Shibuya M, Zeiger DM, Butcher RA, Ragains JR, Clardy J, Touhara K, Sengupta P (2009) Two chemoreceptors mediate developmental effects of dauer pheromone in *C. elegans*. *Science* 326: 994 – 998

Kumari S, Mg S, Mayor S (2010) Endocytosis unplugged: multiple ways to enter the cell. *Cell Res* 20: 256 – 275

Lawe DC, Patki V, Heller-Harrison R, Lambright D, Corvera S (2000) The FYVE domain of early endosome antigen 1 is required for both phosphatidylinositol 3-phosphate and Rab5 binding. Critical role of this dual interaction for endosomal localization. *J Biol Chem* 275: 3699 – 3705

Lawe DC, Chawla A, Merithew E, Dumas J, Carrington W, Fogarty K, Lifshitz L, Tuft R, Lambright D, Corvera S (2002) Sequential roles for phosphatidylinositol 3-phosphate and Rab5 in tethering and fusion of early endosomes via their interaction with EEA1. *J Biol Chem* 277: 8611 – 8617

Lechtreck KF (2015) IFT-cargo interactions and protein transport in cilia. *Trends Biochem Sci* 40: 765 – 778

Li G, D'Souza-Schorey C, Barbieri MA, Roberts RL, Klippel A, Williams LT, Stahl PD (1995) Evidence for phosphatidylinositol 3-kinase as a regulator of endocytosis via activation of Rab5. *Proc Natl Acad Sci USA* 92: 10207 – 10211

Liedtke W, Tobin DM, Bargmann CI, Friedman JM (2003) Mammalian TRPV4 (VR-OAC) directs behavioral responses to osmotic and mechanical stimuli in *Caenorhabditis elegans*. *Proc Natl Acad Sci USA* 100(Suppl 2): 14531 – 14536

Malicki J, Avidor-Reiss T (2014) From the cytoplasm into the cilium: bon voyage. *Organogenesis* 10: 138 – 157

Mangeol P, Prevo B, Peterman EJG (2016) KymographClear and KymographDirect: two tools for the automated quantitative analysis of molecular and cellular dynamics using kymographs. *Mol Biol Cell* 27: 1948 – 1957

Mayinger P (2012) Phosphoinositides and vesicular membrane traffic. *Biochim Biophys Acta* 1821: 1104 – 1113

McBride HM, Rybin V, Murphy C, Giner A, Teasdale R, Zerial M (1999) Oligomeric complexes link Rab5 effectors with NSF and drive membrane fusion via interactions between EEA1 and syntaxin 13. *Cell* 98: 377 – 386

McIntyre JC, Hege MM, Berbari NF (2016) Trafficking of ciliary G protein-coupled receptors. *Methods Cell Biol* 132: 35 – 54

Milenkovic L, Scott MP, Rohatgi R (2009) Lateral transport of Smoothened from the plasma membrane to the membrane of the cilium. *J Cell Biol* 187: 365 – 374

Mills IG, Jones AT, Clague MJ (1998) Involvement of the endosomal autoantigen EEA1 in homotypic fusion of early endosomes. *Curr Biol* 8: 881 – 884

Molla-Herman A, Ghossoub R, Blisnick T, Meunier A, Serres C, Silbermann F, Emmerson C, Romeo K, Bourdoncle P, Schmitt A, Saunier S, Spassky N, Bastin P, Benmerah A (2010) The ciliary pocket: an endocytic membrane domain at the base of primary and motile cilia. *J Cell Sci* 123: 1785 – 1795

Monis WJ, Faundez V, Pazour GJ (2017) BLOC-1 is required for selective membrane protein trafficking from endosomes to primary cilia. *J Cell Biol* 216: 2131 – 2150

Morrison HA, Dionne H, Rusten TE, Brech A, Fisher WW, Pfeiffer BD, Celniker SE, Stenmark H, Bilder D (2008) Regulation of early endosomal entry by the *Drosophila* tumor suppressors Rabenosyn and Vps45. *Mol Biol Cell* 19: 4167 – 4176

Mukhopadhyay S, Badgandi HB, Hwang S-H, Somatilaka B, Shimada IS, Pal K (2017) Trafficking to the primary cilium membrane. *Mol Biol Cell* 28: 233 – 239

Nachury MV, Seeley ES, Jin H (2010) Trafficking to the ciliary membrane: how to get across the periciliary diffusion barrier? *Annu Rev Cell Dev Biol* 26: 59 – 87

Nager AR, Goldstein JS, Herranz-Pérez V, Portran D, Ye F, Garcia-Verdugo JM, Nachury MV (2017) An actin network dispatches ciliary GPCRs into extracellular vesicles to modulate signaling. *Cell* 168: 252 – 263.e14

Naslavsky N, Boehm M, Backlund PS Jr, Caplan S (2004) Rabenosyn-5 and EHD1 interact and sequentially regulate protein recycling to the plasma membrane. *Mol Biol Cell* 15: 2410 – 2422

Navaroli DM, Bellvé KD, Standley C, Lifshitz LM, Cardia J, Lambright D, Leonard D, Fogarty KE, Corvera S (2012) Rabenosyn-5 defines the fate of the transferrin receptor following clathrin-mediated endocytosis. *Proc Natl Acad Sci USA* 109: E471 – E480

Nielsen E, Christoforidis S, Uttenweiler-Joseph S, Miaczynska M, Dewitte F, Wilm M, Hoflack B, Zerial M (2000) Rabenosyn-5, a novel Rab5 effector, is complexed with hVPS45 and recruited to endosomes through a FYVE finger domain. *J Cell Biol* 151: 601 – 612

O'Hagan R, Wang J, Barr MM (2014) Mating behavior, male sensory cilia, and polycystins in *Caenorhabditis elegans*. *Semin Cell Dev Biol* 33: 25 – 33

Papermaster DS, Schneider BG, Besharse JC (1985) Vesicular transport of newly synthesized opsin from the Golgi apparatus toward the rod outer segment. Ultrastructural immunocytochemical and autoradiographic evidence in *Xenopus retinas*. *Invest Ophthalmol Vis Sci* 26: 1386 – 1404

Parton RG, del Pozo MA (2013) Caveolae as plasma membrane sensors, protectors and organizers. *Nat Rev Mol Cell Biol* 14: 98 – 112

Patki V, Virbasius J, Lane WS, Toh BH, Shpetner HS, Corvera S (1997) Identification of an early endosomal protein regulated by phosphatidylinositol 3-kinase. *Proc Natl Acad Sci USA* 94: 7326 – 7330

Peden EM, Barr MM (2005) The KLP-6 kinesin is required for male mating behaviors and polycystin localization in *Caenorhabditis elegans*. *Curr Biol* 15: 394 – 404

Pedersen LB, Mogensen JB, Christensen ST (2016) Endocytic control of cellular signaling at the primary cilium. *Trends Biochem Sci* 41: 784 – 797

Perkins LA, Hedgecock EM, Thomson JN, Culotti JG (1986) Mutant sensory cilia in the nematode *Caenorhabditis elegans*. *Dev Biol* 117: 456 – 487

Phua SC, Chiba S, Suzuki M, Su E, Roberson EC, Pusapati GV, Setou M, Rohatgi R, Reiter JF, Ikegami K, Inoue T (2017) Dynamic remodeling of membrane composition drives cell cycle through primary cilia excision. *Cell* 168: 264 – 279.e15

Rahajeng J, Caplan S, Naslavsky N (2010) Common and distinct roles for the binding partners Rabenosyn-5 and Vps45 in the regulation of endocytic trafficking in mammalian cells. *Exp Cell Res* 316: 859 – 874

Rattner JB, Sciore P, Ou Y, van der Hoorn FA, Lo IKY (2010) Primary cilia in fibroblast-like type B synoviocytes lie within a cilium pit: a site of endocytosis. *Histol Histopathol* 25: 865 – 875

Reiter JF, Blacque OE, Leroux MR (2012) The base of the cilium: roles for transition fibres and the transition zone in ciliary formation, maintenance and compartmentalization. *EMBO Rep* 13: 608 – 618

Reiter JF, Leroux MR (2017) Genes and molecular pathways underpinning ciliopathies. *Nat Rev Mol Cell Biol* 18: 533 – 547

Rohatgi R, Milenkovic L, Scott MP (2007) Patched1 regulates hedgehog signaling at the primary cilium. *Science* 317: 372 – 376

Rosenbaum JL, Witman GB (2002) Intraflagellar transport. *Nat Rev Mol Cell Biol* 3: 813 – 825

Saito M, Otsu W, Hsu K-S, Chuang J-Z, Yanagisawa T, Shieh V, Kaitsuka T, Wei F-Y, Tomizawa K, Sung C-H (2017) Tctex-1 controls ciliary resorption by regulating branched actin polymerization and endocytosis. *EMBO Rep* 18: 1460 – 1472

Sanders AAWM, Kennedy J, Blacque OE (2015) Image analysis of *Caenorhabditis elegans* ciliary transition zone structure, ultrastructure, molecular composition, and function. *Methods Cell Biol* 127: 323 – 347

Sann SB, Crane MM, Lu H, Jin Y (2012) Rabx-5 regulates RAB-5 early endosomal compartments and synaptic vesicles in *C. elegans*. *PLoS One* 7: e37930

Satir P, Pedersen LB, Christensen ST (2010) The primary cilium at a glance. *J Cell Sci* 123: 499 – 503

Sato M, Sato K, Fonarev P, Huang C-J, Liou W, Grant BD (2005) *Caenorhabditis elegans* RME-6 is a novel regulator of RAB-5 at the clathrin-coated pit. *Nat Cell Biol* 7: 559 – 569

Schafer JC, Haycraft CJ, Thomas JH, Yoder BK, Swoboda P (2003) XBX-1 encodes a dynein light intermediate chain required for retrograde intraflagellar transport and cilia assembly in *Caenorhabditis elegans*. *Mol Biol Cell* 14: 2057 – 2070

Schneider CA, Rasband WS, Eliceiri KW (2012) NIH Image to ImageJ: 25 years of image analysis. *Nat Methods* 9: 671 – 675

Schou KB, Pedersen LB, Christensen ST (2015) Ins and outs of GPCR signaling in primary cilia. *EMBO Rep* 16: 1099 – 1113

Schou KB, Mogensen JB, Morthorst SK, Nielsen BS, Aleliunaite A, Serra-Marques A, Fürstenberg N, Saunier S, Bizet AA, Veland IR, Akhmanova A, Christensen ST, Pedersen LB (2017) KIF13B establishes a CAV1-enriched microdomain at the ciliary transition zone to promote Sonic hedgehog signalling. *Nat Commun* 8: 14177

Simonsen A, Lippé R, Christoforidis S, Gaullier JM, Brech A, Callaghan J, Toh BH, Murphy C, Zerial M, Stenmark H (1998) EEA1 links PI(3)K function to Rab5 regulation of endosome fusion. *Nature* 394: 494 – 498

Simpson JC, Joggerst B, Laketa V, Verissimo F, Cetin C, Erfle H, Bexiga MG, Singan VR, Hériché J-K, Neumann B, Mateos A, Blake J, Bechtel S, Benes V, Wiemann S, Ellenberg J, Pepperkok R (2012) Genome-wide RNAi screening identifies human proteins with a regulatory function in the early secretory pathway. *Nat Cell Biol* 14: 764 – 774

Solomon A (2004) *Caenorhabditis elegans* OSR-1 regulates behavioral and physiological responses to hyperosmotic environments. *Genetics* 167: 161 – 170

Somsel Rodman J, Wandinger-Ness A (2000) Rab GTPases coordinate endocytosis. *J Cell Sci* 113(Pt 2): 183 – 192

Starich TA, Herman RK, Kari CK, Yeh WH, Schackwitz WS, Schuyler MW, Collet J, Thomas JH, Riddle DL (1995) Mutations affecting the chemosensory neurons of *Caenorhabditis elegans*. *Genetics* 139: 171 – 188

Szymanska K, Johnson CA (2012) The transition zone: an essential functional compartment of cilia. *Cilia* 1: 10

Troemel ER, Sagasti A, Bargmann CI (1999) Lateral signaling mediated by axon contact and calcium entry regulates asymmetric odorant receptor expression in *C. elegans*. *Cell* 99: 387 – 398

van der Vaart A, Rademakers S, Jansen G (2015) DLK-1/p38 MAP kinase signaling controls cilium length by regulating RAB-5 mediated endocytosis in *Caenorhabditis elegans*. *PLoS Genet* 11: e1005733

Vetter M, Wang J, Lorentzen E, Deretic D (2015) Novel topography of the Rab11-effector interaction network within a ciliary membrane targeting complex. *Small GTPases* 6: 165 – 173

Wang J, Silva M, Haas LA, Morsci NS, Nguyen KCQ, Hall DH, Barr MM (2014) *C. elegans* ciliated sensory neurons release extracellular vesicles that function in animal communication. *Curr Biol* 24: 519 – 525

Wang J, Barr MM (2016) Ciliary extracellular vesicles: txt msg organelles. *Cell Mol Neurobiol* 36: 449 – 457

Waters AM, Beales PL (2011) Ciliopathies: an expanding disease spectrum. *Pediatr Nephrol* 26: 1039 – 1056

Wätzlich D, Vetter I, Gotthardt K, Miertzschke M, Chen Y-X, Wittinghofer A, Ismail S (2013) The interplay between RPGR, PDEδ and Arl2/3 regulate the ciliary targeting of farnesylated cargo. *EMBO Rep* 14: 465 – 472

Williams CL, Li C, Kida K, Inglis PN, Mohan S, Semenec L, Bialas NJ, Stupay RM, Chen N, Blacque OE, Yoder BK, Leroux MR (2011) MKS and NPHP modules cooperate to establish basal body/transition zone membrane associations and ciliary gate function during ciliogenesis. *J Cell Biol* 192: 1023 – 1041

Wood CR, Huang K, Diener DR, Rosenbaum JL (2013) The cilium secretes bioactive ectosomes. *Curr Biol* 23: 906 – 911

Wood CR, Rosenbaum JL (2015) Ciliary ectosomes: transmissions from the cell's antenna. *Trends Cell Biol* 25: 276 – 285